CHARLES UNIVERSITY
FACULTY OF SCIENCE
INSTITUTE OF GEOCHEMISTRY, MINERALOGY
AND MINERAL RESOURCES
&
ARISTOTLE UNIVERSITY OF THESSALONIKI
FACULTY OF SCIENCE
SCHOOL OF GEOLOGY
DEPARTMENT OF MINERALOGY, PETROLOGY AND ECONOMIC GEOLOGY

AGNI CHATZIANTONIOU

A MINERALOGICAL AND GEOCHEMICAL ASSESSMENT OF THE As-, Cu-, In-, Pb-, Sb- AND Zn-RICH MINE WASTES AT PEFKA EPITHERMAL DEPOSIT IN EVROS, GREECE

BACHELOR THESIS

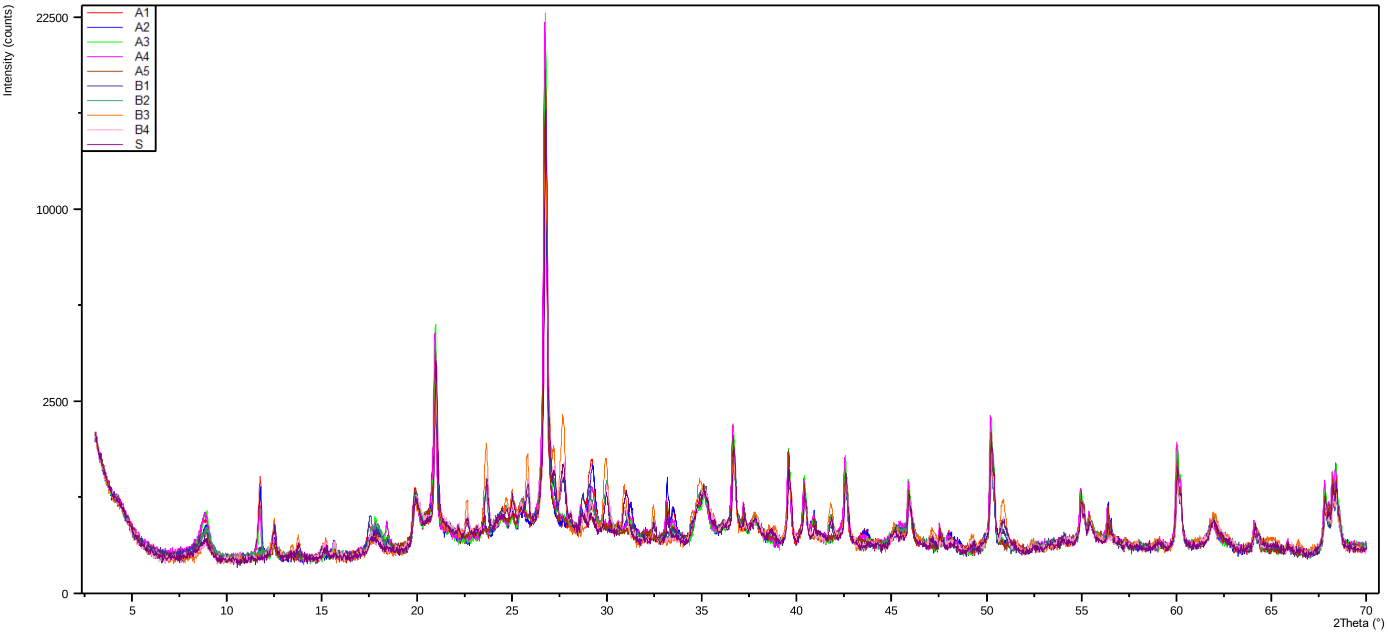

AGNI CHATZIANTONIOU

A mineralogical and geochemical assessment of the As-, Cu-, In-, Pb-, Sb- and Zn-rich mine wastes at Pefka epithermal deposit in Evros, Greece.

The bachelor thesis was submitted at the Department of Geology, Aristotle University of Thessaloniki, Greece

Supervising professors:
Drahota Petr
Melfos Vasilios

A mineralogical and geochemical assessment of the As-, Cu-, In-, Pb-, Sb- and Zn-rich mine wastes at Pefka epithermal deposit in Evros, Greece.

TABLE OF CONTENTS

Abstract

Title: A mineralogical and geochemical assessment of the As-, Cu-, In-, Pb-, Sb- and Zn- rich mine wastes at Pefka epithermal deposit in Evros, Greece.

By: Agni Chatziantoniou (5736)

The Pefka deposit is an intermediate (IS) to high (HS) sulfidation polymetallic deposits of NE Greece. According to the publication by Dimou et al. (1994) which was based on the mineralogical and geochemical alterations of the rocks, the mineralization in the area of Pefka is an epithermal system with a high sulfidation state. Specifically, the mineralization is highly enriched in copper (more than 1 wt%) and indium (around 700 ppm) and is composed by two cross-cutting vein systems with intermediate (IS) and high (HS) sulfidation state, which are found in andesitic lavas (Voudouris et al. 2021). Mining in Pefka, with shafts, underground galleries and surface operations was active during the 1950's, but since then any environmental restoration was not held.

The aim of this research is to analyze the presence of As, Cu, In, Pb, Sb and Zn in the mine wastes of this epithermal system, observe the secondary mineral phases of these elements and evaluate their potential mobility in the waste material. To succeed this, a detailed geochemical and mineralogical study was carried out, by processing ten samples, collected from three different locations of the Pefka area (A1-A5, B1-B4, S). The methods that were used for this study were: geochemical [X-Ray Fluorescence (XRF) analysis, pH measurements, mineralization and quantitative chemical analysis, sequential extraction (SE) analysis] and mineralogical [X-Ray Diffraction (XRD) analysis, Electron Probe Microanalysis (EPMA)]. The sequential extraction, XRD analysis and microprobe analysis were applied for selected samples, which were found by XRF to have special interest, chemically and mineralogically. This multi-method data set was combined to reach the final conclusions.

1. Introduction-Importance of metals in the epithermal systems

Epithermal geological systems refer to a specific type of hydrothermal deposits of minerals, which are configured after the circulation of hot fluids through porous and permeable rocks near the Earth's surface (Pirajno, 2009). These fluids, which are typically rich in metals, such as zinc (Zn), silver (Ag), and gold (Au), can deposit valuable ore minerals. The different compositions and temperatures of the hydrothermal fluids, the host rock types and the style of mineralization, work as factors for discrimination of the epithermal deposits in various types. The most common types of epithermal deposits include high-sulfidation, intermediate-sulfidation, and low-sulfidation deposits, commonly related to porphyry systems (Fig. 1). They are typically found in volcanic and volcanic-associated terrains and are often associated with geothermal systems. These deposits are economically important, as they are the sources of base and precious metals.

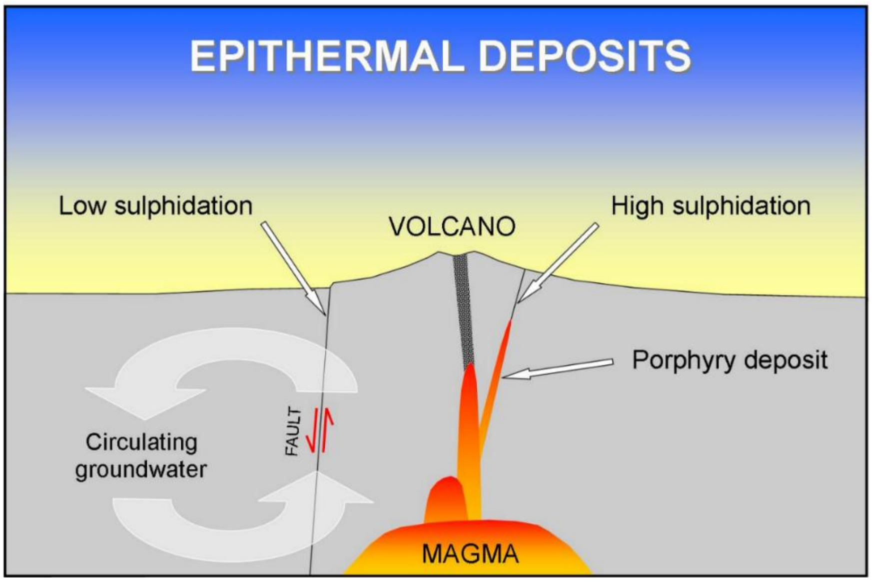

Fig. 1. The procedure of formation of an epithermal system (Tilley, 2021)

Metals play important role in epithermal geological systems as they are commonly related to the formation of these deposits. Epithermal deposits are typically formed by the circulation of hydrothermal fluids, through porous and permeable rocks, and these fluids often contain dissolved metals that can precipitate out to form mineral deposits. Additionally, the structural and mineralogical characteristics of the host rocks can also control the formation and preservation of epithermal deposits. Therefore, the presence of certain metals, such as gold and silver, can be used as indicators of the potential for epithermal mineralization in a given area.

There are several indicators that can be used to identify potential areas for epithermal mineralization in a given area. Some of these indicators include:

Geology: Epithermal deposits are typically associated with volcanic and volcanic-associated terrains, and they can be found in areas with a history of geothermal activity. Therefore, areas with volcanic rocks and geothermal systems are considered prospective for epithermal mineralization.

Alteration: Hydrothermal fluids can alter the composition and texture of rocks, leading to the conformation of distinctive altered minerals such as clay minerals, silica minerals, and sulfides. These alteration minerals can be used as indicators of the presence of epithermal mineralization.

Structures: Epithermal deposits can form along faults, fractures, and other structural features that provide pathways for the circulation of hydrothermal fluids. Therefore, areas with well-developed structural features are considered prospective for epithermal mineralization.

Geochemistry: Epithermal deposits are typically associated with metal-rich fluids, so elevated concentrations of metals such as gold, silver, zinc, and lead in soils and stream sediments can be used as indicators of potential epithermal mineralization in a given area.

Remote sensing: The hydrothermal alteration and mineralization associated with epithermal deposits can affect the spectral properties of rocks, making it possible to detect the potential for epithermal mineralization using remote sensing techniques such as satellite imagery and aerial photography.

It is worth to note that these indicators are not unique to epithermal deposits and can be associated with other types of mineralization, so it's important to consider multiple lines of evidence when assessing the potential for epithermal mineralization in a given area.

2. Geology and base metal mineralization of the Rhodope Massif

The Rhodope massif in Greece (Fig. 2) is known for its rich mineral deposits, including base metal mineralization (Melfos and Voudouris et al. 2017, Voudouris et al. 2021). The geology of the area is characterized by a complex tectonic setting and a long history of magmatism and metamorphism, due to the orogenic and post-orogenetic conditions. The Rhodope Massif is a geological unit, which is located in the Balkan Peninsula, spanning across Bulgaria and Greece. It is a complex and highly metamorphosed terrain that was formed during the Paleozoic and Mesozoic eras as a result of multiple tectonic events, including the closure of the Paleo-Tethys Ocean and the subsequent collision of several microplates and continents. The massif is currently bounded by several major faults and is characterized by a diverse array of lithologies and structural features.

The Rhodope massif is divided into three subdomains , which are separated from each other by the Nestos thrust fault and are the Northern Rhodope Domain, the Southern Rhodope Core Complex, and the Chalkidiki Block (Panagopoulos and Papanikolaou, 1981). The Northern Rhodope Domain is composed by three main metamorphic units, including a lower unit of high-grade basement and four metamorphic core complexes, an intermediate unit of high-grade basement rocks, which have relations with ocean and continental crusts, and underwent a high-grade amphibolite-facies overprinted by a high to ultra-high-pressure metamorphism, and an uppermost Mesozoic low-grade unit of the Evros ophiolite and the Circum-Rhodope Belt. The Southern Rhodope Core Complex (SRCC) consists of Permo-Carboniferous orthogneiss, and Triassic marbles, which are incorporated in amphibolitic and metapelitic rocks. The Chalkidiki Block is a thrust system that comprises four NW-trending units, the Vertiskos Unit, the Circum-Rhodope Belt, the Chortiatis Magmatic Suite, and the eastern Vardar ophiolites.

The Vertiskos Unit consists of a Silurian-Ordovician peraluminous orthogneiss fragment, which interpolates with rocks like paragneiss, marble, amphibolite, eclogite, and serpentinite. The Thermes-Volvi-Gomati (TVG) complex separates the Vertiskos Unit from the Southern Rhodope Kerdylion Unit and includes the Athos-Volvi Suture Zone and mafic- ultramafic rocks. The Circum-Rhodope Belt unit is composed of low-grade metasedimentary and metavolcanic rocks of Triassic-Jurassic protolith age.

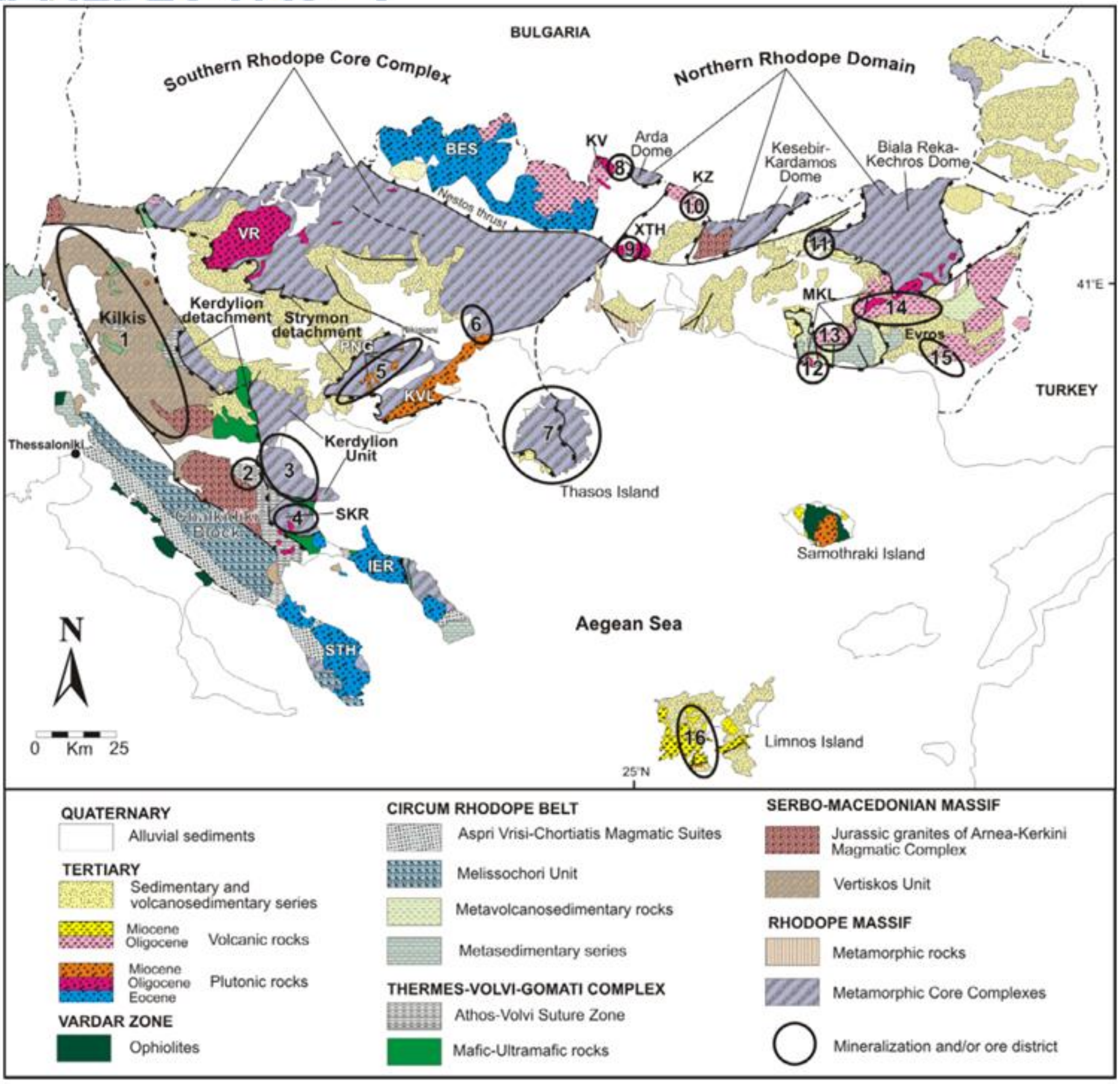

Fig. 2. Geological map of the Rhodope Massif and the Vertiskos Unit in the northern Greek regions, with the main- tectonic units, the location of the main detachments and the mineralization and/or ore districts (Melfos and Voudouris, 2017). N°15 shows the mineralization of Evros (Pefka).

The Rhodope Mountains, located in northern Greece (Fig. 3), are composed of metamorphic rocks that have been affected by intense tectonic activity. The area is characterized by a numerous north-south trending fault zones, which are of great importance in the formation and preservation of mineral deposits. The most important mineralization in the Rhodope is the base metal deposits of Olympias and Stratoni in Chalkidiki. These deposits contain lead, zinc, gold, and silver, and were formed from the hydrothermal activity associated with the regional magmatism and tectonics. The area is primarily composed of metamorphic rocks, including schists, gneisses, amphibolites, and marbles, which have undergone multiple episodes of deformation and metamorphism. The mineralization in the Rhodope Mountains is associated with Cenozoic magmatism and includes intrusion related, skarn, carbonate replacement, porphyry, epithermal, and vein-type deposits (Melfos and Voudouris et al. 2017, Voudouris et al. 2021), characterized by the presence of sulfide minerals such as pyrite, chalcopyrite, and sphalerite.

The Evros region (NRD) in northeastern Greece is characterized by a different geology, with the presence mainly of carbonates, volcanoclastics and volcanic rocks (Ashworth K. L., 1988). The mineralization in the Evros region is primarily magmatic hydrothermal, associated with igneous, plutonic, subvolcanic, and volcanic rocks. These deposits are characterized by the presence of sulfide minerals such as pyrite, chalcopyrite, galena, and sphalerite with variable concentration of Au, Ag, and rare metals. They have an Oligocene-Miocene age and are represented mainly by porphyry and epithermal style of mineralization.

The Evros-Rhodope region is primarily composed of metamorphic rocks, including schists, phyllites, and meta-quartzites, which have undergone multiple episodes of deformation and metamorphism. The area is also characterized by the presence of intrusions of igneous rocks such as monzonite, granodiorite, diorite, and granite, and a variety of volcanic rocks, including andesite, dacite and rhyolite.

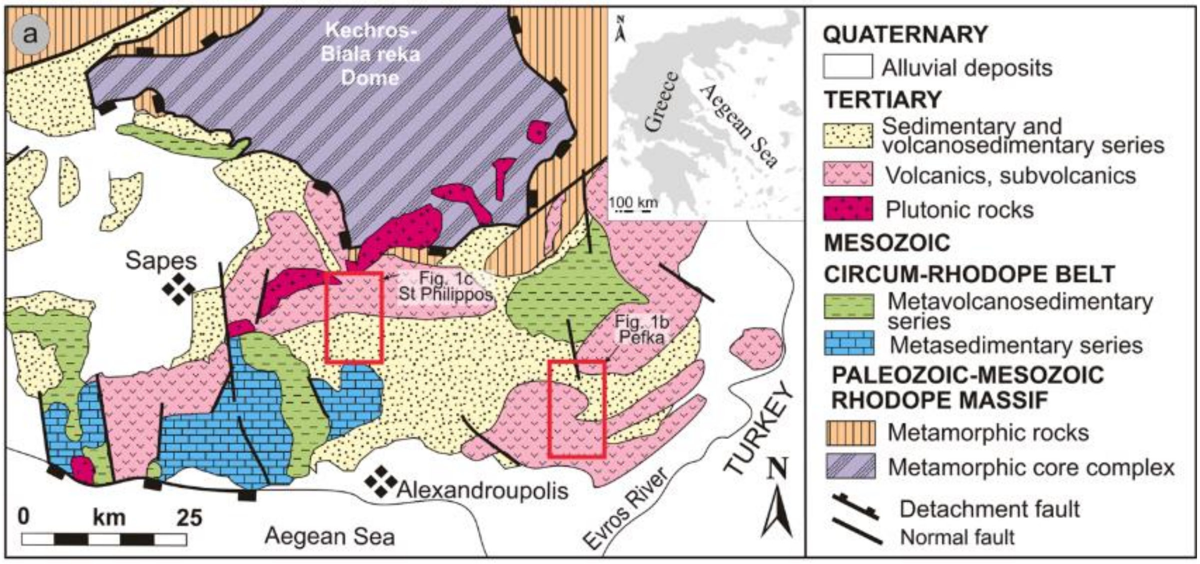

Fig. 3. Geological map of the SE region of Rhodope with the location of the deposit of Pefka (Voudouris et al.,2021)

The epithermal deposits are associated with volcanic activity and are characterized by the presence of sulfide minerals such as pyrite, chalcopyrite, and sphalerite.

3. Region of Pefka

3.1. Geology of the region

The geology of the area of Pefka-Loutra basin (Fig. 4), consists of pyroclastic and sedimentary rocks of an Upper Eocene- Oligocene age, and volcanic rocks of an Oligocene to Miocene age. These rocks have an intermediate to felsic calc alkaline character. The volcanic activity was associated with two mafic and two felsic stages, resulting in pyroclastic and lava flows, domes, and tuffs. The characteristic intermediate (IS) to high (HS) sulfidation epithermal system of Pefka (Voudouris et al., 2021) is associated to alkaline rocks in the south (Lofos of Pasas), to more acidic volcanic rocks, such as rhyodacites and dacites, in the rest of the area (Michael, 2004).

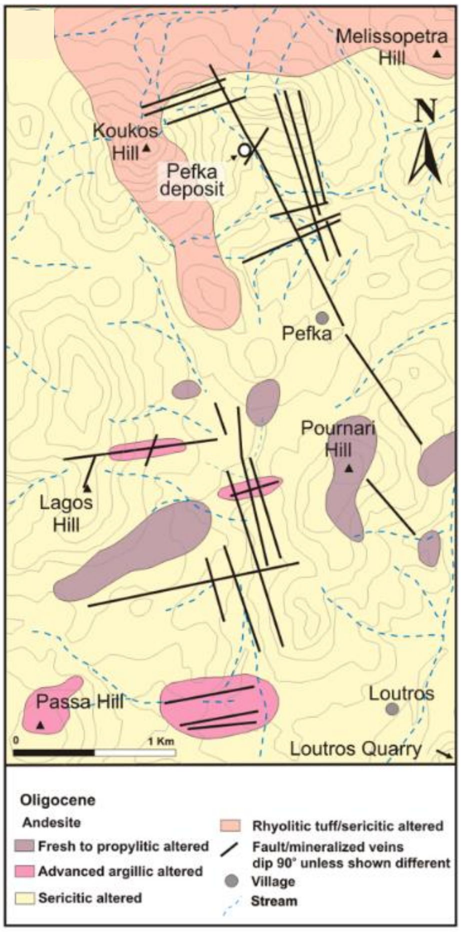

Fig. 4. Geological map of Pefka (Voudouris et al., 2021)

3.2. The epithermal system of Pefka

In the region of Pefka, the formations are characterized by chemical and mineralogical alterations similar to the Kassiteres-Konos area (Arikas and Voudouris, 1998). Two sulfidation stages in the epithermal systems were detected, a high and a low. The alterations in the high-sulfidation epithermal system show a vertically and horizontally – laterally zoning. These alterations include an inner silicic zone, an intermediate part, which is an advanced argillic alteration that changes progressively, in sericitic-propylitic at the outer area. As for the vertical zonation, an advanced argillic alteration is developed below the silicic zone, and it alters downwardly to sericitic and intermediate argillic alterations (Voudouris et al., 2021).

Mineralogically, the silicic alteration is present with two types, vuggy and massive silica (Voudouris et al., 2021). These types of alterations are found along faults or in their intersections. The vuggy silica type consists of fine-grained quartz with minor amounts of alunite, anatase, and pyrite. The massive silica variety is composed of microcrystalline quartz, abundant pyrite, as well as chalcopyrite. The argillic alteration consists of two types, an inner quartz and alunite assemblage, and an outer quartz and kaolinite-dickite (+ alunite) assemblage. (Voudouris et al., 2021).

The high-sulfidation veins were formed in the rocks that consist of these two alternations. The veins consist of aggregates of alunite, barite, and chalcedony. Below the advanced argillic and silicic zones, there are low-sulfidation quartz and calcite veins with K-feldspar, sericitic and intermediate argillic alteration. Because the low-sulfidation quartz veins go through the silicic bodies, they postdate the high-sulfidation acid leaching.

The development of highly silicified rocks, which are composed mainly of quartz and minor alunite, was caused by an early stage hypogene acid leaching.

According to the publication of Dimou et al. (1994), which was based on the mineralogical and geochemical alterations of the rocks, the mineralization in the area of Pefka is categorized as a high-sulfidation epithermal system and contains two different types (Fig. 5). The first one is an early NNW-trending type, which consists of high-sulfidation veins of quartz, and Au-enargite-luzonite, and the second one is a NE trending type, with intermediate sulfidation veins of carbonates and breccias that host tennantite and tellurides. Sericitic to argillic alteration of the host rock wraps the veins of the first mineralization type, and minerals like sericite and barite are found in these veins.

The intermediate argillic alteration envelops the veins of the second type of Pefka mineralization. Some high level fragments of the telluride-carbonate veins corrupt and form bulk and wide calcite, which is hosted in limp masses around the mine and higher levels of topography. According to the publication of Melfos and Voudouris et al. (2012), the bulk samples of both types of Pefka mineralization contain up to 10 ppm Au, 25 ppm Mo, 100 ppm Bi, 470 ppm Te, 680 ppm In, 17 ppm Ga, 6 ppm Ge, >100 ppm Ag, >1 wt.% Cu and >1 wt.% As.

The epithermal alteration and mineralization in the area of Pefka is observed in silicic and advanced argillic outcrops found in E-trending faults in the southwestern area. These positions in the fault area transition outward and downward to sericitic and argillic alteration. Silicic and sericite-adularia alteration is located on Koukos Hill, and the silicification connects to a stock room of epithermal-style colloform quartz-chalcedony banded veins.

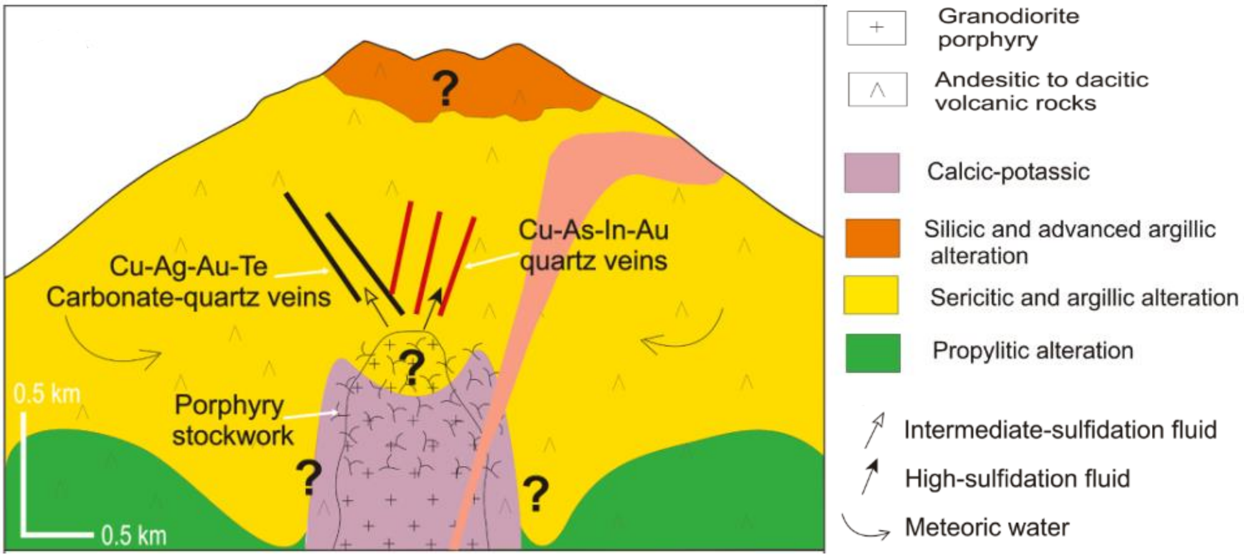

Fig. 5. Diagram of the processing of the mineralization at the deposit of Pefka (Voudouris et al.,2021).

4. Study site

Based on recent studies by Voudouris et al. (2021), the Pefka deposit is an intermediate (IS) to high (HS) sulfidation polymetallic deposit, consisted of breccia and high grade veins. Mining in Pefka, with shafts, underground galleries and surface operations was active during the 1950’s but since then any environmental restoration was not held. The sampling and studying area are located on the east slope of Koukos Hill (Fig. 4), about 1.5 km north of Pefka village and approximately 15 km northeast of the city of Alexandroupolis.

5. Materials and methods

5.1. Sample collection and processing

The material from the mining waste dumps was sampled in two outcrops along the steep side slopes of a small (A) and a large (B) waste pile in an area of approximately 10x10m^2 (Fig. 6a,b). The waste samples (n = 9) were collected along each profile in discrete depth intervals (15 cm in outcrop A; 50-90 cm in outcrop B) distinguished visually from other parts of the profiles. One sample was collected in a shallow excavation pit (S) from the sediment of intermittent stream (Fig. 6c), located approximately 5m downstream of the small waste dump (Table 1). The samples were packed in polyethylene bags and transported to the laboratory.

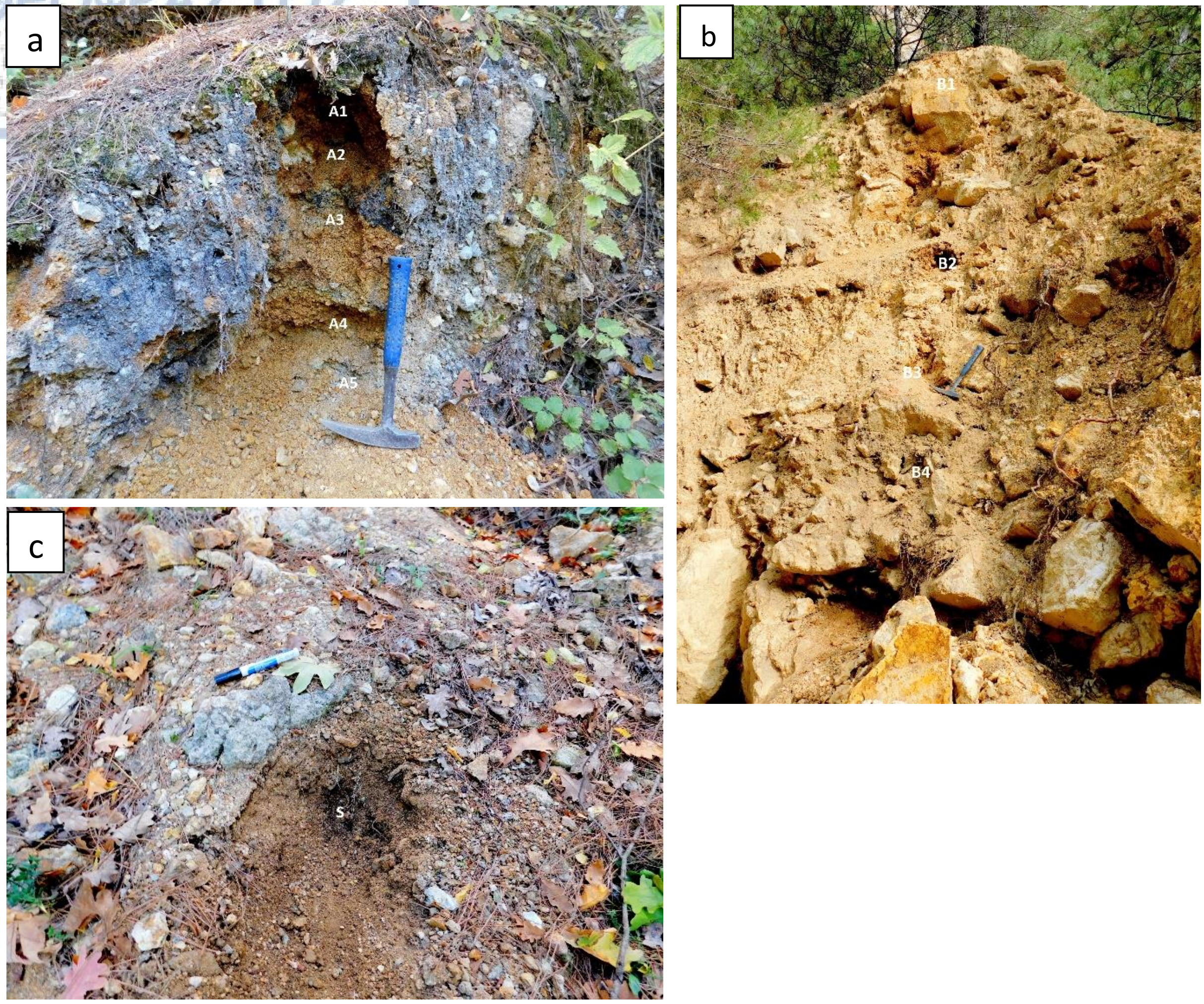

Fig. 6. Sampling sites: **a**. small pile of waste material (profile A), **b**. large pile and possible landslide (profile B), **c**. pit in the sediments of the stream (sediment S).

In the laboratory (Fig.7), the samples were air-dried for 48 hours in a drying and heating chamber (BINDER) with a temperature of 40°C and sieved to obtain <2 mm fraction.

For bulk chemical analysis, a split subsample was grounded in an agate ball mill (Retsch) to analytical fineness. Each sample was processed for 20 minutes with 320 rates per minute (rpm).

The color of the dry materials was also determined using a Munsell soil color chart (Table 1).

Fig. 7. Equipment of the laboratory and procedures of processing the samples: **a.** drying and heating chamber, **b.** 2mm fraction sieve, **c.** agate grinding ball, **d.** equipment of milling procedure, **e.** Munsell soil color chart, **f.** samples after sieving and milling procedures

Table 1. Physical parameters of the studied mining waste and sediment samples

Sample	Depth (cm)	<2 mm (%)	Color
A1	0-15	9	7.5YR 6/6 reddish yellow
A2	15-25	19	7.5YR 7/6 reddish yellow
A3	25-35	17	7.5YR 6/6 reddish yellow
A4	35-45	35	7.5YR 6/8 reddish yellow
A5	45-60	37	7.5YR 7/8 reddish yellow
B1	0-90	32	7.5YR 6/8 reddish yellow
B2	90-140	10	7.5YR 7/6 reddish yellow
B3	140-190	9	10YR 7/4 very pale brown
B4	190-240	30	5YR 5/4 reddish brown
S	0-20	29	7.5YR 4/4 brown

6. Geochemical analysis

6.1. X-ray Fluorescence (XRF) analysis

The milled mining waste samples were analyzed for total element concentration and variety by a Thermo Scientific Niton XL3t x-ray tube-based x-ray analyzer. Every sample was analyzed three times and the semi-quantitative chemical analysis was performed by the parallel processing of a NIST 2711a standard reference material (Montana ΙΙ Soil, moderately elevated trace element concentration) (Fig. 8).

The interpretation of the measurements for each one of the samples, by calculating the averages and standard deviations of the resulting values, showed that the highest values of the interesting elements such as As, Cu, Zn, Pb, In were concentrated in the samples A2 from the profile A, B4 from the profile B and in the sediment S. These three samples will be observed analytically in the following chemical and mineralogical procedures.

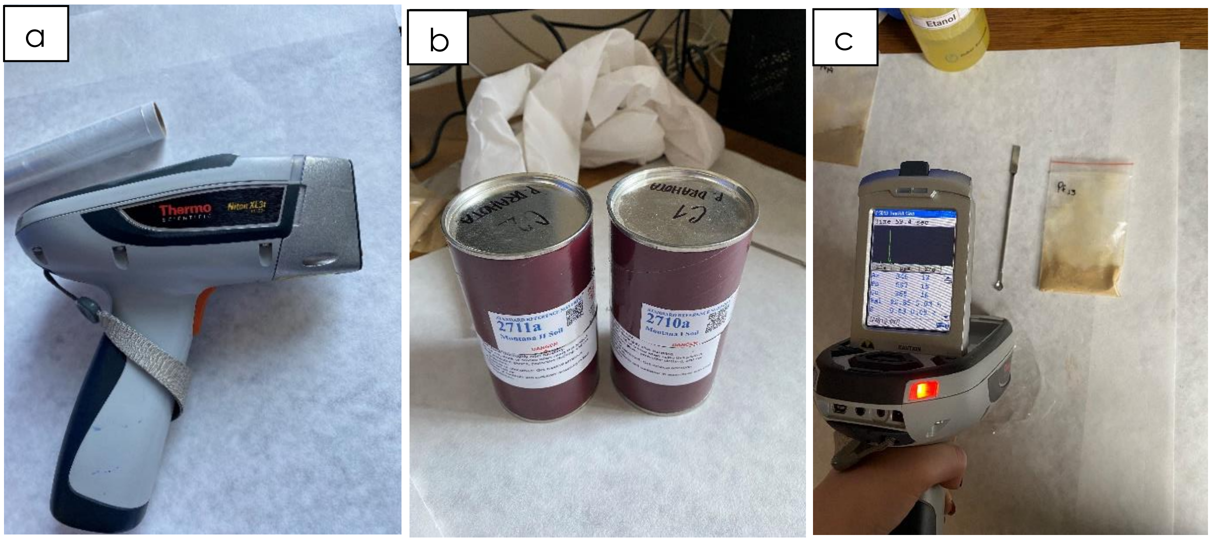

Fig. 8. XRF equipment: **a**. Thermo Scientific Niton XL3t x-ray analyzer, **b**. reference material Montana II Soil, **c**. XRF analyses procedure

6.2. PH measurement

The pH was measured for standardized slurries following reaction of 5 g of dried sample with 25 mL deionized water for 1 hour in a horizontal shaker (Pansu and Gautheyrou, 2006). After 30 minutes of decantation, the pH of the supernatants was measured using a WTW multimeter and combined electrode (SenTix41) with two-point calibration, using standard WTW buffer solutions at pH 4.006 and 6.865 (Fig. 9). The use of the buffers aims to a wider measurement range of the pH of the samples.

Fig. 9. Equipment and procedures of the pH measurement: **a.** weight of dried samples, **b.** horizontal shaker, **c**. WTW multimeter and combined electrode, **d.** buffers

The pH values at the profile A and the profile B, as they are presented in table 2, show that the samples A1-A5 and B1-B4 have an acidic character, which indicates that profiles A and B have been affected by the sulfide oxidation. On the other hand, the sediment S presents near-neutral character which points out the presence of carbon in this sampling area.

Table 2. PH measurement of the mining waste and sediment samples in the H_2O solution.

Sample	**Depth (cm)**	**<2 mm (%)**	**pH_{H20}**
A1	0-15	9	3.28
A2	15-25	19	4.00
A3	25-35	17	3.79
A4	35-45	35	3.87
A5	45-60	37	3.89
B1	0-90	32	3.66
B2	90-140	10	3.67
B3	140-190	9	3.68
B4	190-240	30	4.25
S	0-20	29	6.72

6.3. Mineralization of samples and quantitative chemical analysis

6.3.1. Total sulfur (s_{tot}) and total organic carbon (TOC)

The contents of the total sulfur (S_{tot}), total organic carbon (TOC), and total inorganic carbon (TIC) (Table 3) were determined by using a combination of ELTRA CS 530 and ELTRA CS 500 TIC analyzers (ELTRA, Germany). The ELTRA is widely used for analyzing solid materials and light metals by burning them in high temperatures. In this way, it detects gases like CO_2 and SO_2 (Fig. 10). The ratio of total organic carbon and total inorganic carbon is presented in table 4.

Table 3. Total organic carbon (TOC) and total sulfur (S_{tot}) percentages after the ELTRA analysis.

Sample	Carbon %	Sulfur %
A1	0.21	2.41
A2	0.2	3.53
A3	0.12	1.75
A4	0.18	2.03
A5	0.28	1.95
B1	0.25	1.14
B2	0.65	0.86
B3	0.18	0.59
B4	0.47	0.67
S	1.64	0.91

Table 4. Ratio of total organic carbon and total inorganic carbon (TOC)/(TIC).

Sample	Depth	<2 mm	TOC/TIC
	(cm)	(%)	(g/kg)
A1	0-15	9	2.1/bdl
A2	15-25	19	2.0/bdl
A3	25-35	17	1.2/bdl
A4	35-45	35	1.8/bdl
A5	45-60	37	2.8/bdl
B1	0-90	32	2.5/bdl
B2	90-140	10	6.5/bdl
B3	140-190	9	1.8/bdl
B4	190-240	30	4.7/bdl
S	0-20	29	16.2/0.16

TOC - total organic carbon; TIC - total inorganic carbon; bdl - below detection limit of 0.1 g/kg

6.3.2. Trace elements, metals, and metalloids

For the determination of the major and trace elements, an acid digestion procedure was used. An amount of 0.2 g of each sample (Table 5) was dissolved in a Pt dish in a mixture of 10 mL of HF (49% v/v) and 0.5 mL of $HClO_4$ (70% v/v) on a hot plate (450°C). The mixture was, then, evaporated to near-dryness and the procedure was repeated with 5 mL of HF and 0.5 mL of $HClO_4$. The residue was then dissolved in 2% HNO_3 (v/v) and diluted to 100 mL before the analysis. The results are given in table 6.

Table 5. Total weights of the acid digestion procedure of the samples before and after the heating.

Sample	Weight of the beaker (g)	Weight of the sample (g)	Total weight (g)	Total weight after heating (g)	Rest (g)
A5	26.3435	0.2001	26.5436	26.5334	0.1898
A4	26.8819	0.2001	27.0820	27.0713	0.1894
A3	26.6732	0.2004	26.8736	26.8637	0.1905
A2	26.6675	0.1999	26.8674	26.8553	0.1878
A1	24.8803	0.1996	25.0799	25.0678	0.1875
B4	26.7504	0.2002	26.9506	26.9402	0.1898
B3	27.5230	0.2003	27.7233	27.7148	0.1918
B2	27.8085	0.2003	28.0088	27.9947	0.1862
B1	25.9937	0.1998	26.1935	26.1800	0.1863
S	25.8025	0.1998	26.0023	25.9909	0.1884
NIST 2711a	35.1530	0.1998	35.3528	35.3438	0.1908

Table 6. Trace elements in the mining waste and sediment samples. All data are in mg/kg.

Sample	Depth (cm)	Ag	Ba	Bi	Co	Ga	Ge	Mo	Ni	Sn	Te	Tl	V
A1	0-15	2.31	510	0.668	3.01	20.8	0.787	1.43	2.27	4.37	0.961	3.21	55
A2	15-25	2.71	417	0.775	5.22	20.2	0.757	1.36	6.50	5.09	0.557	3.61	60.6
A3	25-35	4.28	382	0.821	2.14	29.6	0.980	1.41	4.11	5.98	0.816	3.17	79.3
A4	35-45	4.13	368	0.894	3.24	24.2	0.829	1.56	5.03	5.25	0.714	3.31	73.2
A5	45-60	3.98	301	0.828	4.1	24.4	0.890	2.04	4.99	6.62	0.461	3.78	77.8
B1	0-90	2.72	1060	0.767	2.32	17.0	0.585	1.67	6.26	2.44	4.18	7.03	87.5
B2	90-140	2.62	749	0.470	1.41	15.1	0.303	2.13	7.83	2.17	2.5	5.02	127
B3	140-190	0.836	660	0.163	0.468	12.3	0.425	1.36	3.57	2.09	1.25	3.93	93.2
B4	190-240	5.33	519	0.486	18.6	13.6	0.813	1.89	6.18	2.44	4.18	7.03	87.5
S	0-20	2.86	737	0.290	15.8	12.1	0.825	1.57	9.08	2.15	0.483	6.08	69.3

The concentrations of metals and metalloids (Ag, Al, As, Ba, Bi, Ca, Co, Cu, Fe, Ga, Ge, In, K, Mg, Mo, Mn, Ni, Sb, Sn, Te, Tl, V, Zn) were determined by using either an inductively coupled plasma optical emission spectrometry (ICP-OES, Agilent 5110, USA) or a quadrupole-based inductively coupled plasma mass spectrometry (ICP-MS, Thermo Scientific, iCAP-Q$^{\text{TM}}$, Germany) (Fig. 10). The results are presented in table 7.

Table 7. Concentrations of metals and metalloids after the use of ICP-OES and ICP-MS spectrometry procedures.

Sample	**Depth**	**<2 mm**	**S**	**K**	**Na**	**Ca**	**Mg**	**Al**	**Fe**	**Mn**	**As**	**Cu**	**In**	**Pb**	**Sb**	**Zn**
	(cm)	**(%)**	**mg/kg**													
A1	0-15	9	24.1	23.4	2.46	18.3	5.22	65.8	46.4	798	203	563	3.47	1460	200	1490
A2	15-25	19	35.3	23.3	2.13	21.7	5.91	70.6	47.5	1310	221	1920	3.22	1420	317	768
A3	25-35	17	17.5	20.9	2.20	6.61	4.51	65.1	43.6	324	242	1290	10.5	2270	405	578
A4	35-45	35	20.3	21.7	2.22	9.03	5.08	70.8	42.8	611	251	1510	8.69	1670	403	830
A5	45-60	37	19.5	23.5	2.74	5.62	5.35	75.2	49.4	709	230	1410	4.12	1850	320	905
B1	0-90	32	11.4	36.1	6.21	1.48	5.13	89.8	56.6	417	496	670	0.76	854	385	140
B2	90-140	10	8.6	38.9	6.44	0.24	3.81	94.6	38.5	246	433	617	3.36	803	478	250
B3	140-190	9	5.9	50.7	8.40	0.47	2.62	88.5	22.3	75	229	354	1.32	229	223	57
B4	190-240	30	6.7	39.4	18.2	0.53	3.51	84.8	34.4	2480	638	1230	5.10	1180	687	163
S	0-20	29	9.1	35.5	17.7	5.36	5.42	71.2	35.4	3020	252	649	0.48	630	181	972

All the chemicals, which were used during the digestion procedure, were reagent-grade (Merck-Sigma-Aldrich, Germany), and deionized water, obtained from a Millipore Academic system (Millipore, USA), was used for the dilutions. The ratio of the quality control/quality assurance (QA/QC) (Table 8) of the bulk digestion procedure and subsequent analysis was performed again by the parallel processing of an NIST 2711a standard reference material (Montana II Soil, moderately elevated trace element concentration) and was found to be satisfactory.

Tables 8A, 8B. Quality control/quality assurance (QA/QC) results (mean standard ± deviation) for the NIST 2711a reference material. ([a]: information value, n.p: not provided).

A **Element**	**Mass Fraction**	**Measured** $n = 2$	**Certified**
Al	%	6.25±0.05	6.72±0.06
Ca	%	2.08±0.03	2.42±0.06
Fe	%	2.80±0.03	2.82±0.04
K	%	2.46±0.01	2.53±0.10
Mg	%	0.98±0.04	1.07±0.06
Na	%		1.20±0.01
Ag	mg/kg	4.98±0.05	6[a]
As	mg/kg	99±3	107±5
Ba	mg/kg	542±10	730±15
Bi	mg/kg	1.24±0.02	n.p.
Co	mg/kg	8.5±0.1	9.89±0.18
Cu	mg/kg	134±2	140±2

B **Element**	**Mass Fraction**	**Measured n=2**	**Certified**
Ga	mg/kg	12.2±0.3	n.p.
Ge	mg/kg	1.3±0.1	n.p.
In	mg/kg	0.883±0.001	1[a]
Mn	mg/kg	667±12	675±18
Mo	mg/kg	1.14±0.01	n.p.
Ni	mg/kg	18.6±0.4	21.7±0.7
Pb	mg/kg	1420±30	1400±10
Sb	mg/kg	22.4±0.3	23.8±1.4
Sn	mg/kg	4.6±0.2	n.p.
Te	mg/kg	0.42±0.03	n.p.
Tl	mg/kg	2.37±0.05	3[a]
V	mg/kg	74±1	80.7±5.7
Zn	mg/kg	417±9	414±11

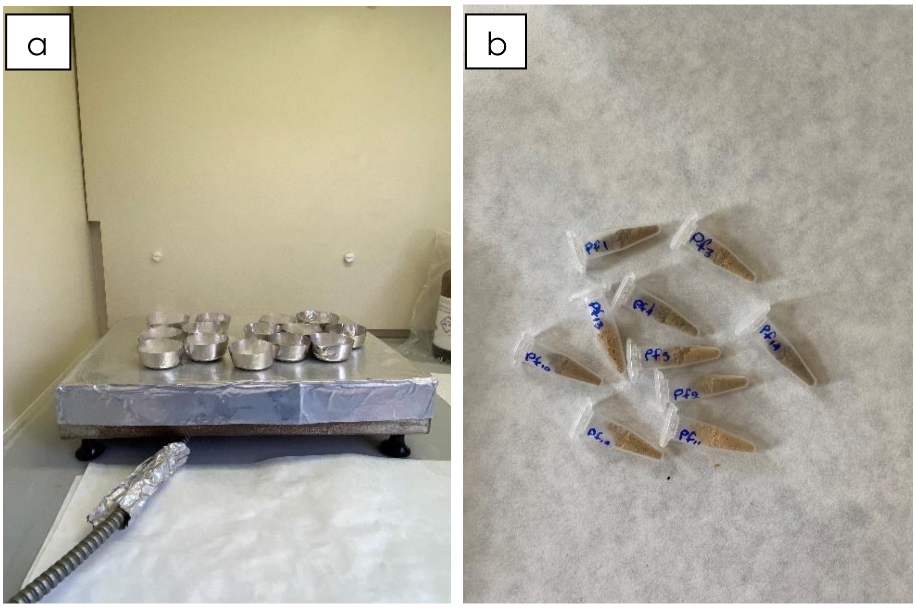

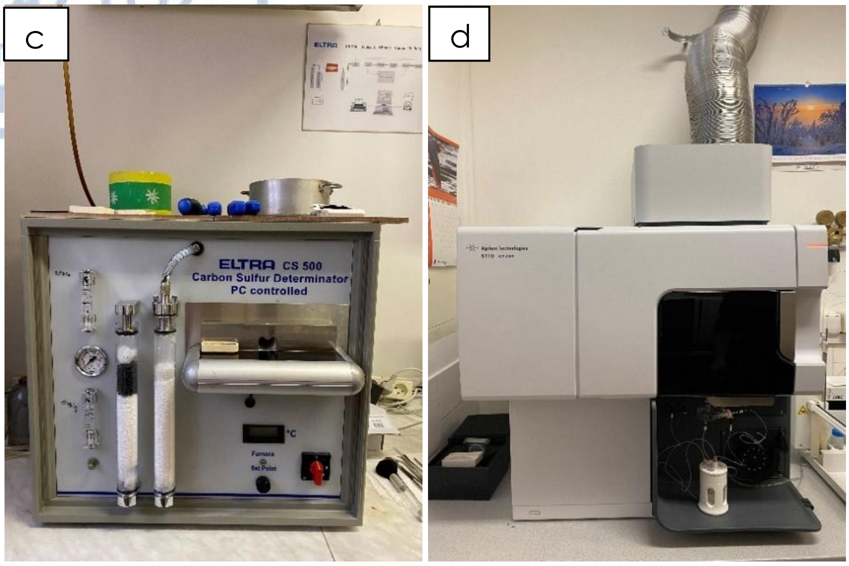

Fig. 10. Equipment for the process of mineralization of the samples: **a.** heating of the samples, **b.** samples for the ELTRA analyzing procedure, **c.** ELTRA CS 500 TIC analyzer, **d.** ICP-OES 5100 analyzer.

6.4. Sequential extraction analysis (SE)

Sequential extraction (SE) procedure is a laboratory technique, used to study the partitioning and mobility of elements in solid samples such as soils, sediments, and rocks (Passos et al., 2010). The technique involves a series of selective chemical extractions, in which, different fractions of the sample are extracted under specific conditions designed to target different forms of elements. The sequential extraction analysis is based on the principle that different chemical species of an element may have different chemical properties and may have varying environmental behavior. By extracting and analyzing the different fractions separately, the sequential extraction analysis provides information on the availability, mobility, and potential toxicity of elements in a sample.

For this study, to observe the dissolution of the secondary phases of As, Cu, In, Pb, Sb, Zn and a potential mobility of these elements in the waste material, each of the <2mm samples was subjected to a four-step sequential extraction (SE) analysis. The target of the SE was to quantify specific chemical fractions of selected metals and metalloids (Table 9):

- (F1) water-soluble fraction
- (F2) absorbed and exchangeable fraction
- (F3) poorly crystalline Fe(III) (hydr)oxides and hydroxysulfates fraction
- (F4) crystalline Fe(III) (hydr)oxides, hydroxysulfates and arsenates fraction

Table 9: Sequential extraction sequence applied in this study.

Fraction	**Extractant**	**Extraction conditions**	**SSR**	**Preferentially dissolved fraction**	**References**
F1	deionized H_2O	24 h, RT	1:50	Water-soluble sulfates	Dold 2003; Drahota et al. 2014
F2	1 M NH_4-acetate, pH 7	2 h, RT	1:100	Adsorbed and exchangeable ions	Ure 1996
F3	0.2 M NH_4-oxalate/oxalic acid, pH 3	2 h, RT, dark	1:100	X-ray amorphous Fe (oxyhydr)oxides, hydroxysulfates, arsenates	Dold 2003; Drahota et al. 2014
F4	0.2 M NH_4-oxalate/oxalic acid, pH 3	4 h, 80 °C	1:100	Crystalline Fe (oxyhydr)oxides, hydroxysulfates, arsenates	Dold 2003; Drahota et al. 2014
SSR - solid solution ratio; **RT** - room temperature					

Step 1: Water-soluble fraction (F1)

A quantity of 0.5gr of each sample reacted with 25mL deionized water for 24 hours in a horizontal shaker (Pansu and Gautheyrou, 2006) in room temperature (RT) with speed 100 rates/minute. The water extracts (F1) were measured for pH, Eh and e.c (Table 10), in room temperature of approximately 25^oC. For the pH measurement a WTW multimeter was used and a combined electrode (SenTix41) with two-point calibration, using standard WTW buffer solutions at pH 4.006 and 6.865. For the Eh measurement a WTW multimeter was used (Fig. 11c) and the performance of the combined redox electrode (SenTix, ORP, WTW) was verified by using fresh Zobell's solution (Nordstrom, 1997). After the pH, Eh and electric conductivity measurements, the samples were centrifugated at 8000 rates per minute (rpm) for five minutes (Fig. 11b) , were filtered by using a nylon 0.2 μm filter and acidified by adding 1M HNO_3.

A quantity of 10mL of each sample (Fig. 11e) was analyzed by using a 1.10-phenanthroline and DR 3900 spectrophotometer for the determination of Fe(II) and Fe(III) species in a detection area of 0.2-6.0mg/L (Fig. 11f). The concentrations of Fe species in each sample were found to be below the detection limit. The major anions (Br^-, Cl^-, NO_3^-, PO_4^{3-}, SO_4^{2-}) were measured (Table 11) by using a Dionex ICS-2000 chromatography system (Dionex, USA).

Table 10. Measurements of potential of hydrogen (pH), electrical potential (Eh) which describes the oxidation phase of the trace elements and electrical conductivity (e.c).

Samples	pH	Eh (mV)	e.c (mS/cm)
A1	3.867	487	1580
A2	4.558	400.7	1400
A3	4.073	438.9	846
A4	4.193	399.5	813
A5	4.245	374	580
B1	4.066	473	161
B2	3.970	454.7	124
B3	4.034	461	76
B4	4.624	450.5	38.5
S	7.270	284	48

According to table 10, the profile A and the profile B appear to have acidic pH, in contrast to the sediment S which presents neutral pH (like the pH measurement procedure of chapter 6.2). The electrical conductivity of the profile A is much higher than the one of profile B, fact that indicates that the profile A and especially the samples A1, A2 might concentrate a significant amount of Ca, element which appears in gypsum and other sulfate minerals and could be dissolved after the step 1 of the sequential extraction. This assessment is going to be verified after the XRD analysis of the samples.

Table 11. Analysis of the major anions after the water extraction.

Sample	F-	Cl-	Br-	SO_4^{2-}	NO_3-	PO_4^{3-}
	mg/L					
A5	0.50	2.82	<0,2	229	0.26	<0,4
A4	0.38	3.48	<0,2	344	0.48	<0,4
A3	0.45	0.54	<0,2	368	0.21	<0,4
A2	0.39	0.60	<0,2	732.00	0.45	<0,4
A1	0.31	0.45	<0,2	851	0.34	<0,4
B4	0.10	0.57	<0,2	8.52	0.28	<0,4
B3	0.22	0.45	<0,2	12.9	0.15	<0,4
B2	0.52	0.81	<0,2	29.1	0.49	<0,4
B1	0.22	0.90	<0,2	46.5	0.15	<0,4
S	0.22	0.61	<0,2	7.76	0.89	<0,4

Step 2: Absorbed and exchangeable fraction (F2)

For the second step, 77.8gr of NH_4-accetate (Fig. 11g) were dissolved in 1L of deionized water. A quantity of 0.5gr of each sample reacted with 50mL of the liquid mixture for 2 hours in the horizontal shaker and the extraction conditions of Step 1. Then, the samples were centrifugated at 8000 rates per minute (rpm) for five minutes , were filtered by using a nylon 0.2 μm filter and acidified by adding 1M $HNO_{3.}$

Step 3: Poorly crystalline Fe(III) (hydr)oxides and hydroxysulfates fraction (F3)

For the third step, 16.15 g of acid ammonium oxalate $(COONH_4)2H_2O^3$ and 10.9 g of oxalic acid $(COOH)_2,2H_2O_4$ were dissolved in approximately 1000mL of deionized water. A quantity of 0.5gr of each sample reacted with 50mL of the liquid mixture for 2 hours in the horizontal shaker, in room temperature, after it was fully covered with aluminium foil to succeed the requisite darkness. Then, the samples were centrifugated at 8000 rates per minute (rpm) for five minutes and filtered by using a nylon 0.2 μm filter, as in the previous steps. The B4 sample, after the shaking, was found to have a light pink tone.

Step 4: Crystalline Fe(III) (hydr)oxides, hydroxysulfates and arsenates fraction (F4)

For the last step, 16.15 g of acid ammonium oxalate $(COONH_4)_2H_2O_3$ and 10.9 g of oxalic acid $(COOH)_2,_2H_2O_4$ were dissolved in approximately 1000mL of deionized water. A quantity of 0.5gr of each sample reacted with 50mL of the liquid mixture and each testing tube was heated at 80^{o}C for four hours (Fig. 11h). Then, the samples were manually shaken and centrifugated at 8000 rates per minute (rpm) for five minutes. Finally, they filtered by using a nylon 0.2 μm filter. At the end of the step 4, the samples were observed to have green tone, which possibly indicates the dissolution of a significant amount of Fe.

Fig. 11. Equipment used at the SE procedures: **a.** weight scale of the samples, **b.** benchtop centrifuge (UNIVERSAL 320R, Hettich), **c.** WTW multimeter and redox electrode for Eh measurement, **d.** processing of the samples after the centrifugation, **e.** 10mL testing tubes for Fe^{2+} and Fe^{3+} determination, **f.** DR 3900 spectrophotometer for the determination of Fe^{2+} and Fe^{3+} species, **g.** NH4-accetate used for the F2 fraction, **h.** heating of the samples at 80°C for the F4 fraction.

Table 12 presents the final concentrations of the elements of interest for this study, after the four steps of the sequential extraction:

Table 12. Extractability of Fe, Cu, Pb, Zn, In, As and Sb in the sequential extraction (values in mg/kg).

	A1	**A2**	**A3**	**A4**	**A5**	**B1**	**B2**	**B3**	**B4**	**S**
H_2O										
Fe	1.1	0.4	0.8	<0.25	0.4	0.2	1.2	1.1	<0.25	8.3
Cu	70 (12)	120 (6)	94 (7)	76 (5)	77 (5)	100 (15)	66 (11)	29 (8)	60 (5)	0.8 (0.1)
Pb	16 (3)	7.2 (2)	7.2 (2)	5.1 (2)	1.7 (2)	0.1 (2)	0.04 (0.5)	0.1 (0.2)	0.04 (0.6)	0.1 (2)
Zn	45 (3)	54 (7)	26 (5)	26 (3)	26 (3)	5.9 (4)	11 (4)	3.0 (5)	4.1 (3)	0.4
In	<0.0005	<0.0005	<0.0005	<0.0005	<0.0005	<0.0005	<0.0005	<0.0005	<0.0005	<0.0005
As	<0.04	<0.04	<0.04	<0.04	<0.04	<0.04	<0.04	<0.04	<0.04	<0.04
Sb	<0.15	<0.15	<0.15	<0.15	<0.15	<0.15	<0.15	<0.15	1.5 (0.2)	11 (6)
1M NH_4-acetate, pH 7										
Fe	<0.5	<0.5	<0.5	<0.5	<0.5	<0.5	<0.5	<0.5	<0.5	<0.5
Cu	6.4 (1)	52 (3)	18 (1)	18 (1)	21 (2)	20 (3)	15 (2)	5.7 (2)	87 (7)	14 (2)
Pb	15 (1)	14 (1)	9.9 (0.4)	5.3 (0.3)	1.3 (0.1)	0.04	0.03	0.06	0.3	1.0 (0.2)
Zn	0.6	1.1 (0.1)	0.4 (0.1)	0.4	0.5	0.3 (0.2)	0.3 (0.1)	0.2 (0.3)	0.6 (0.3)	9.7 (1)
In	<0.001	<0.001	<0.001	<0.001	<0.001	<0.001	<0.001	<0.001	<0.001	<0.001
As	<0.07	<0.07	<0.07	<0.07	<0.07	<0.07	<0.07	<0.07	<0.07	<0.07
Sb	2.9 (1)	2.7 (1)	3.6 (1)	2.6 (1)	2.3 (1)	1.8 (0.5)	2.8 (0.6)	1.5 (0.7)	4.0 (0.6)	3.7 (2)
NH_4-oxalate/oxalic acid, pH 3, darkness										
Fe	5200 (11)	7020 (15)	9660 (22)	5110 (12)	9110 (18)	8440 (15)	4020 (10)	4360 (20)	2130 (6)	4110 (12)
Cu	68 (12)	660 (34)	250 (19)	280 (19)	310 (22)	110 (17)	88 (14)	45 (13)	520 (42)	370 (58)
Pb	140 (9)	96 (7)	160 (7)	270 (16)	58 (3)	5.3 (1)	2.9 (0.4)	0.6 (0.2)	25 (2)	86 (14)
Zn	21 (1)	74 (10)	17 (3)	15 (2)	24 (3)	6.2 (4)	3.4 (1)	1.7 (3)	13 (8)	350 (36)
In	0.4 (12)	1.1 (34)	3.7 (35)	1.8 (21)	1.3 (32)	0.10 (13)	0.52 (16)	0.23 (18)	1.1 (21)	0.1 (29)
As	32 (16)	53 (24)	70 (29)	31 (12)	54 (23)	96 (19)	69 (16)	30 (13)	142 (22)	55 (22)
Sb	44 (22)	80 (25)	124 (31)	55 (14)	90 (28)	60 (16)	27 (6)	11 (5)	40 (6)	27 (15)
NH_4-oxalate/oxalic acid, pH 3, 80 °C, light										
Fe	38600 (83)	21900 (46)	29200 (67)	25200 (59)	29900 (60)	37000 (65)	22400 (58)	17300 (78)	17600 (51)	15200 (43)
Cu	388 (69)	720 (38)	682 (53)	868 (57)	684 (48)	294 (44)	209 (34)	120 (34)	318 (26)	150 (23)
Pb	1120 (77)	625 (44)	1160 (51)	772 (46)	825 (45)	153 (16)	92 (11)	35 (15)	143 (12)	162 (26)
Zn	83 (6)	163 (21)	64 (11)	70 (8)	85 (9)	25 (18)	19 (8)	7.7 (14)	43 (16)	191 (20)
In	2.2 (68)	1.8 (56)	4.7 (45)	3.5 (40)	2.1 (50)	0.34 (45)	1.3 (38)	0.63 (47)	2.0 (39)	0.19 (40)
As	153 (75)	121 (55)	168 (70)	124 (49)	137 (60)	332 (67)	250 (58)	150 (66)	361 (57)	110 (44)
Sb	100 (50)	109 (34)	179 (44)	128 (32)	139 (43)	192 (50)	190 (40)	102 (46)	356 (52)	36 (20)

[extractability values in parentheses calculated as a percentage of the total concentration; only percentages ≥ 0.1 are included]

The chemical fractionation of the elements of interest, Cu, Pb, Zn, In, As, Sb, was also obtained for the mine waste (A, B) and the sediments (S) by the sequential extraction procedure, and the results are presented in figure 12:

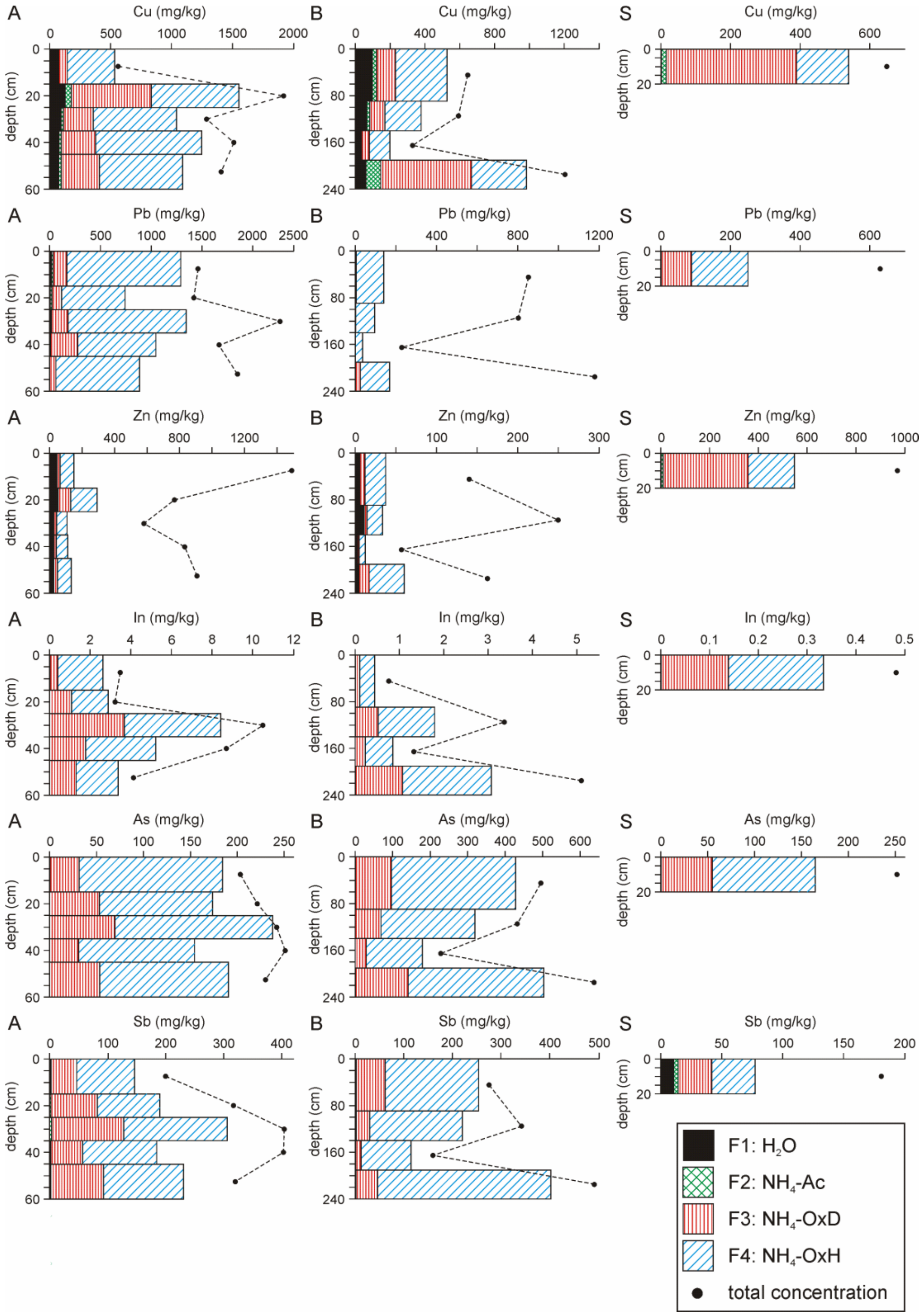

Fig. 12. Chemical fractionation of Cu, Pb, Zn, In As, and Sb in the mining waste (A, B) and sediments (S) samples obtained by sequential extraction procedure. NH_4-Ac: ammonium acetate, NH_4-OxD: ammonium oxalate, darkness, NH_4-OxH: ammonium oxalate, 80 °C, light.

Conclusions of the chemical fractionation based on figure 12

Results of the sequential extraction reveal characteristic disproportion in the mobility of the elements in the first two extractions F1, F2, compared to the F3 and F4. From the water-soluble fraction (F1) only small amounts of copper (Cu), zinc (Zn), and lead (Pb) at profiles A, B, and antimony (Sb) at sediment S, are released. The NH_4-accetate fraction (F2) is widely used for the determination of exchangeable elements (mainly absorbed). It is observed that from the (F2) fraction only a small amount of Cu is liberated at profiles A and B, fact that could possibly indicate the replacement of an exchangeable element with Cu, as a result of the sulfide oxidation that takes place in the mine waste. All the other elements seem extremely immobile in the NH_4-accetate. That low mobility of the elements in the first two extractions could indicate their tight binding in the mine waste.

Especially for Pb and Zn, and according to their total concentrations, it becomes clear that they stay insoluble by a large percentage after all four steps of SE. Yet, for their soluble parts, the highest mobility is observed in the last extraction, the NH_4-oxalate fraction in high temperature (F4) in profiles A, B. In the sediment S, Pb and Zn dissolve partly in the NH_4-oxalate fraction in darkness (F3) and partly in the NH_4-oxalate fraction in high temperature (F4). From the other hand, In, As and Sb dissolve to a large extent in the fractions F3 and F4. As is mostly liberated by the NH_4-oxalate fraction in high temperature (F4) in both profiles A, B, and in the sediment S, indicating that it is primarily associated with well-crystalline Fe (hydr)oxides, hydroxysulfates, and arsenates. The association of As with amorphous or poorly crystalline Fe mineral phases (F3) is also obvious in A, B, and S. Significant amounts of As are released at profile B with the highest one to be spotted in B4 sample. The liberation of As and Sb after the operation of NH_4-oxalate fraction in darkness (F3) and NH_4-oxalate fraction in high temperature (F4) could be related to the dissolution of jarosite minerals (Fig.15) at these steps of sequential extraction. Under oxidizing acid conditions, jarosite can react with Fe, dissolve, and lead to the increase of Sb mobility. At the same time, As can be repartitioned to the poorly crystalline Fe(III)-associated phases.

7. Mineralogical analysis

7.1. X-ray Diffraction (XRD) analysis of the bulk mine waste samples

XRD analysis is a common technique used to identify the mineralogy of bulk mine waste samples (Epp, 2016). It can also provide information about the crystal structure and grain size of the minerals present, which can help in predicting their reactivity and potential for weathering or dissolution.

For the mineralogical analysis, the mineralogical composition of the bulk mine waste samples and some individual mineral grains in the <2mm fraction, selected by hand-sorting, were assessed by X-Ray Diffraction, using a PANalytical X´Pert Pro diffractometer (PANalytical, the Netherlands) (Fig. 13a), which was equipped with a X´Celerator multichannel detector (Fig. 13d), with Cu Kα radiation at 40 kV, 30 mA, over the range 3-70° 2theta, with a step of 0.02° and counting time of 150sec per step. The diffraction data were, then, analyzed by X´Pert HighScore Plus 3.0 software, coupled with an ICDD PDF-2 database.

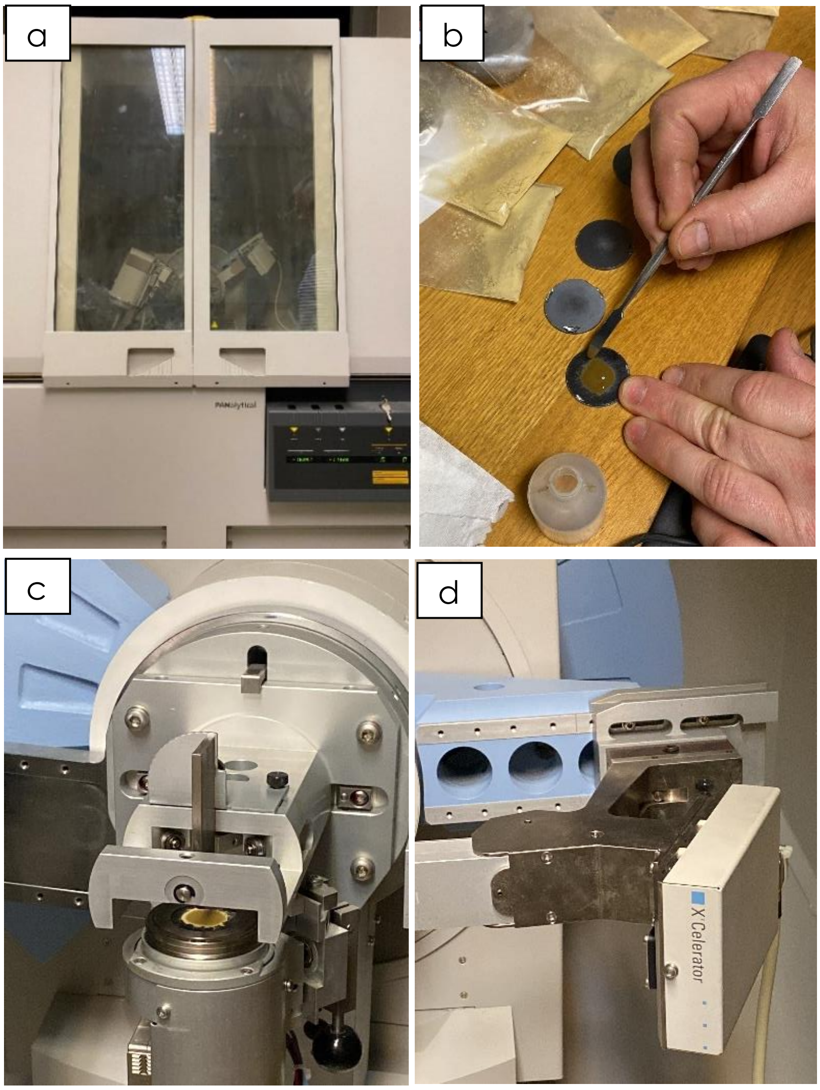

Fig. 13. XRD equipment and procedure: **a.** PANalytical X’Pert Pro diffractometer, **b.** sections with the bulk mine waste, **c.** powder specimen in the diffractometer, **d.** X’Celerator multichannel detector.

7.1.1. Results of XRD analysis of the bulk samples

According to figure 14, the dominant mineral of the profiles A, B, and the sediment S, is quartz (sharp peaks). Significant amounts of clay minerals also appear in both profiles and in the sediment such as kaolinite (Kln), muscovite and/or illite (Ms/Ilt). In the profile A, the samples that are closer to the surface of the outcrop (A4, A5), are composed with minerals of the jarosite group, in contrast to the A5 whose concentration in jarosite seems to fade. The gradual formation of jarosite is an indicator of sulfide oxidation. Specifically, iron sulfides like pyrite are unstable in acidic conditions and oxidize easily to sulfate minerals. The presence of gypsum, a calcium sulfate mineral in the profile A, is another good indicator of the oxidizing conditions. In pattern B, the appearance of jarosite minerals, in combination with the on-site observation of the outcrop in the field, leads to the inference that the profile B constitutes a landslide. In the pattern of the sediment S, the broadening in the peaks in some points, points out the poorly crystalline phase of the minerals. In addition to the presence of pyrite and the neutral pH of the S (6.72 from pH measurement), its safe enough to conclude that this mineral is ferrihydrite and was formed by the oxidation of the Fe(II) with the contribution of the near neutral pH.

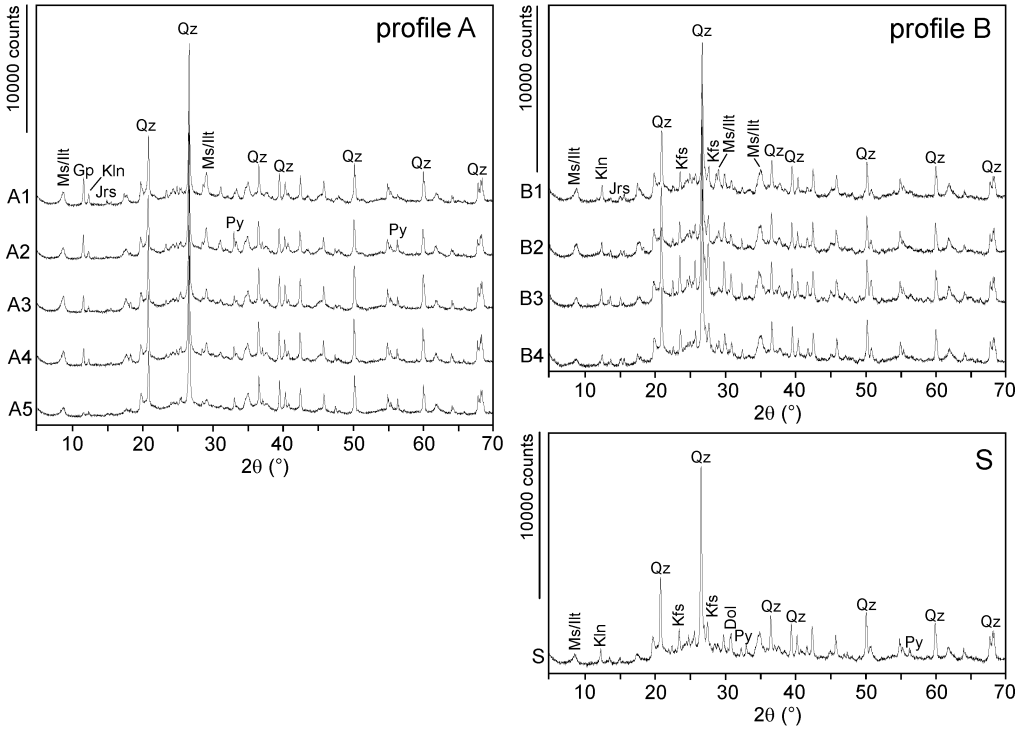

Fig. 14. X-ray diffraction patterns of bulk mining waste (profiles A and B) and sediment (S) samples (<2 mm). **Dol:** dolomite, **Gp:** gypsum, **Jrs:** minerals of jarosite group, **Kfs:** K-feldspar, **Kln:** kaolinite, **Ms/Ilt:** muscovite and/or illite, **Py:** pyrite, **Qz:** quartz.

7.2. X-ray diffraction (XRD) analysis in the sequential extraction

An X-Ray Diffraction (XRD) analysis was also employed after the sequential extraction procedure (SE) for three selected powdered samples A2, B4 and the sediment S, which were found to have the greatest interest geochemically and mineralogically. The XRD analysis was held to test the selectivity of the extractants for major crystalline phases occurring in the mining waste and sediment samples and to determine which minerals went into solution in each step of the sequential extraction.

7.2.1. Results of XRD analysis in the SE

In sample A2 (Fig. 15), gypsum (Gp) was identified with XRD to be totally dissolved after step 1 of the sequential extraction, the water-soluble fraction (F1). In sample B4 and in the sediment S (Fig. 15), the minerals of jarosite group (Jrs) were identified to be partly dissolved after step 3 of the sequential extraction, the poorly crystalline Fe(III) (hydr)oxides and hydroxysulfates fraction (F3), in the hot NH_4-oxalate leach.

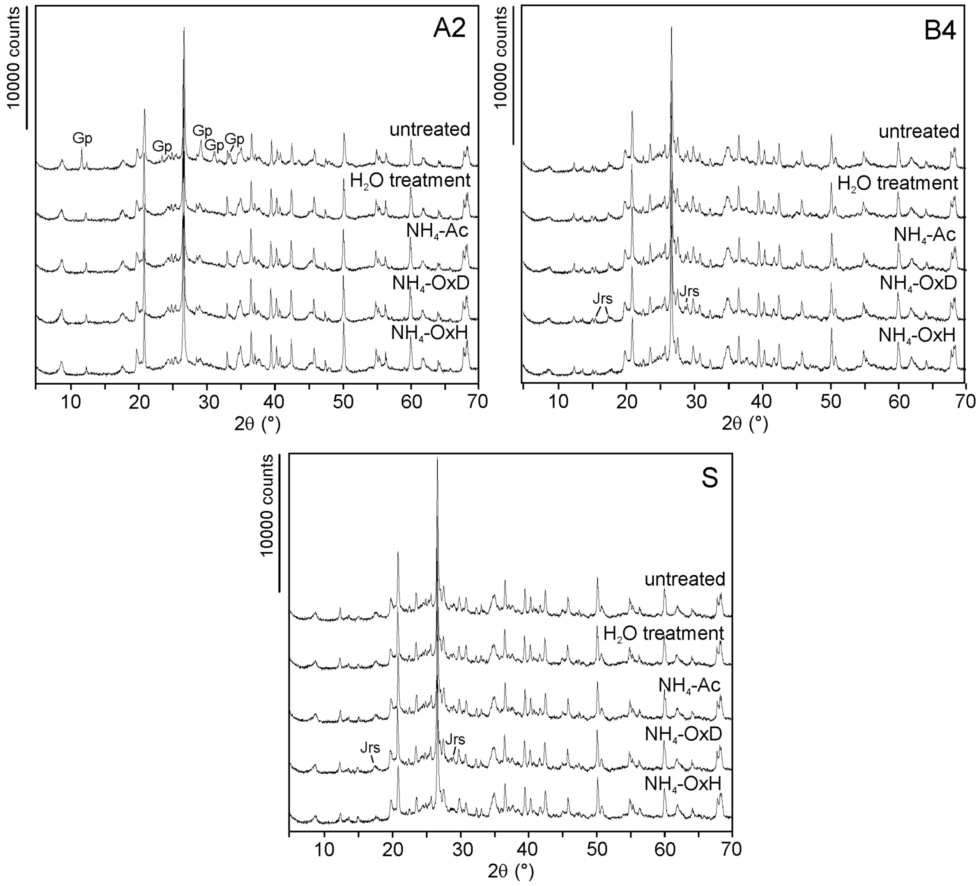

Fig. 15. X-ray diffraction patterns of selected samples (A2, B4 and S) after the four steps of sequential extraction. Gypsum **(Gp)** dissolves in the water treatment (A2); minerals of jarosite group **(Jrs)** dissolve in the hot NH_4-oxalate leach (B4 and S). **NH_4-Ac:** ammonium acetate, **NH_4-OxD:** ammonium oxalate, darkness, **NH_4-OxH:** ammonium oxalate, 80 °C, light.

7.3. Electron Probe Microanalysis (EPMA)

The Electron Probe Microanalysis (EPMA) or "microprobe" is a technique used to determine the elemental composition of a sample, typically in the form of a thin section or polished surface. The technique uses an electron beam to excite the atoms in the sample, causing them to emit characteristic X-rays, which are detected and used to identify the elements present (Castaing, 1960).

For this study, selected bulk samples and heavy-grain concentrates were prepared for Electron Probe Microanalysis in the form of polished sections. Selected samples were A2, B4, and the sediment S (Fig. 16). After the polished thin sections were prepared in the laboratory, they were first examined under a Zeiss Stemi 305 Stereo Microscope for the detection of their secondary phases (Fig. 17). Then, a JEOL JXA-8530F (JEOL, JAPAN) electron probe microanalyzer (EPMA), which was equipped with a field emission gun source (FEG), energy dispersion spectrometer (EDS; JEOL JED-2300F), and five wave-dispersion spectrometers (WDS), was used for the scanning electron microscopic imaging (SEM), Energy-Dispersive X-ray Spectroscopy (EDS) analysis, and quantitative analysis.

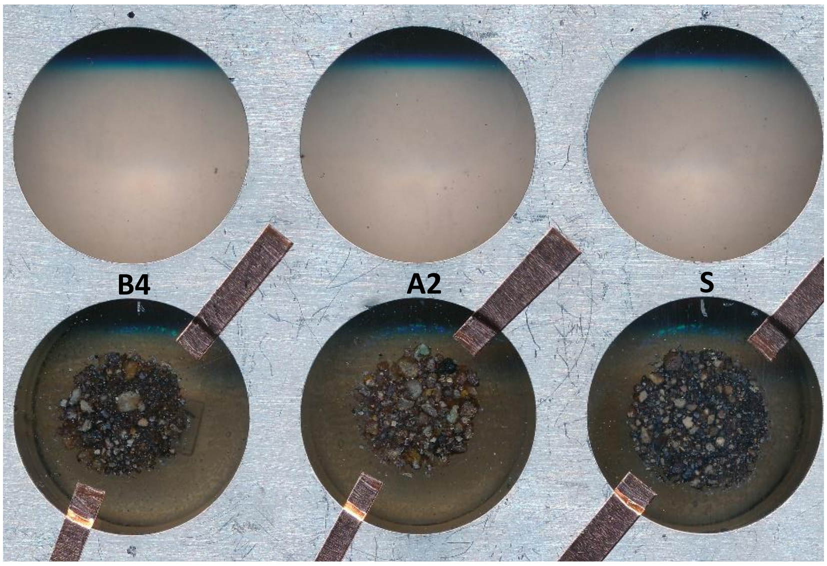

Fig. 16. Polished sections of the samples A2, B4, S under the Zeiss Stereo Microscope.

Fig. 17. Zeiss Stereo Microscope used for the detection of the secondary phases in samples A2, B4, S in the form of polished sections.

The detailed analytical conditions, standards and detection limits used for the EPMA measurements are given in table 13.

Table 13. EPMA conditions, standards, and detection limits.

Element	X-ray	Crystal	Standard	DL (wt.%)
Al	Ka	TAP	Al_2O_3	0.011
P	Ka	TAP	Apatite	0.020
As	La	TAP	Gallium arsenide	0.014
K	Ka	PETJ	Sanidine	0.015
Ca	Ka	PETJ	Apatite	0.012
S	Ka	PETJ	Sphalerite	0.016
Sb	La	PETJ	Stibnite	0.029
Ti	La	PETJ	Rutile	0.023
Pb	Ka	PETJ	Galena	0.024
Fe	Ma	PETJ	Magnetite	0.029
Mn	Ka	LIFL	Rhodonite	0.019
Cu	Ka	LIFL	Cuprite	0.020
Zn	Ka	LIFL	Willemite	0.023
Na	Ka	LIFL	Albite	0.016
Si	Ka	TAP	Quartz	0.016
Mg	Ka	TAP	MgO	0.008
Accelerating voltage 15 kV, beam current 30 nA				

7.3.1. Results of Electron Probe Microanalysis (EPMA)

Specific areas of each sample were analyzed with EPMA and those with the greatest interest are presented in the following figures.

In sample A2, the areas A-J (Fig. 18) were analyzed under the electron probe microanalyzer and the most interesting mineralogically were C, E, G, and H (Fig. 19).

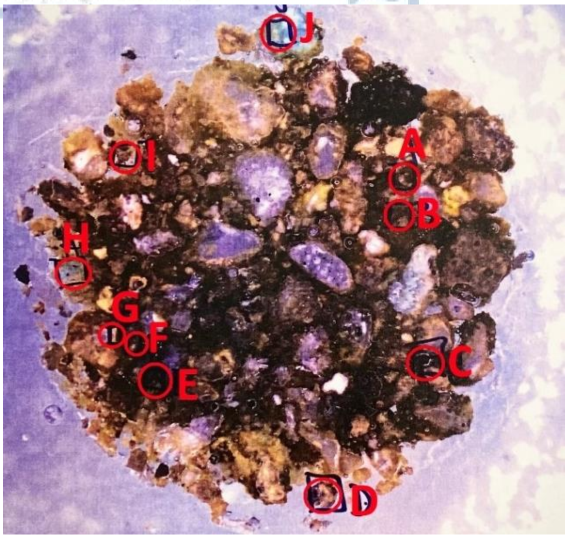

Fig. 18. Sample A2: The analyzed areas A-J.

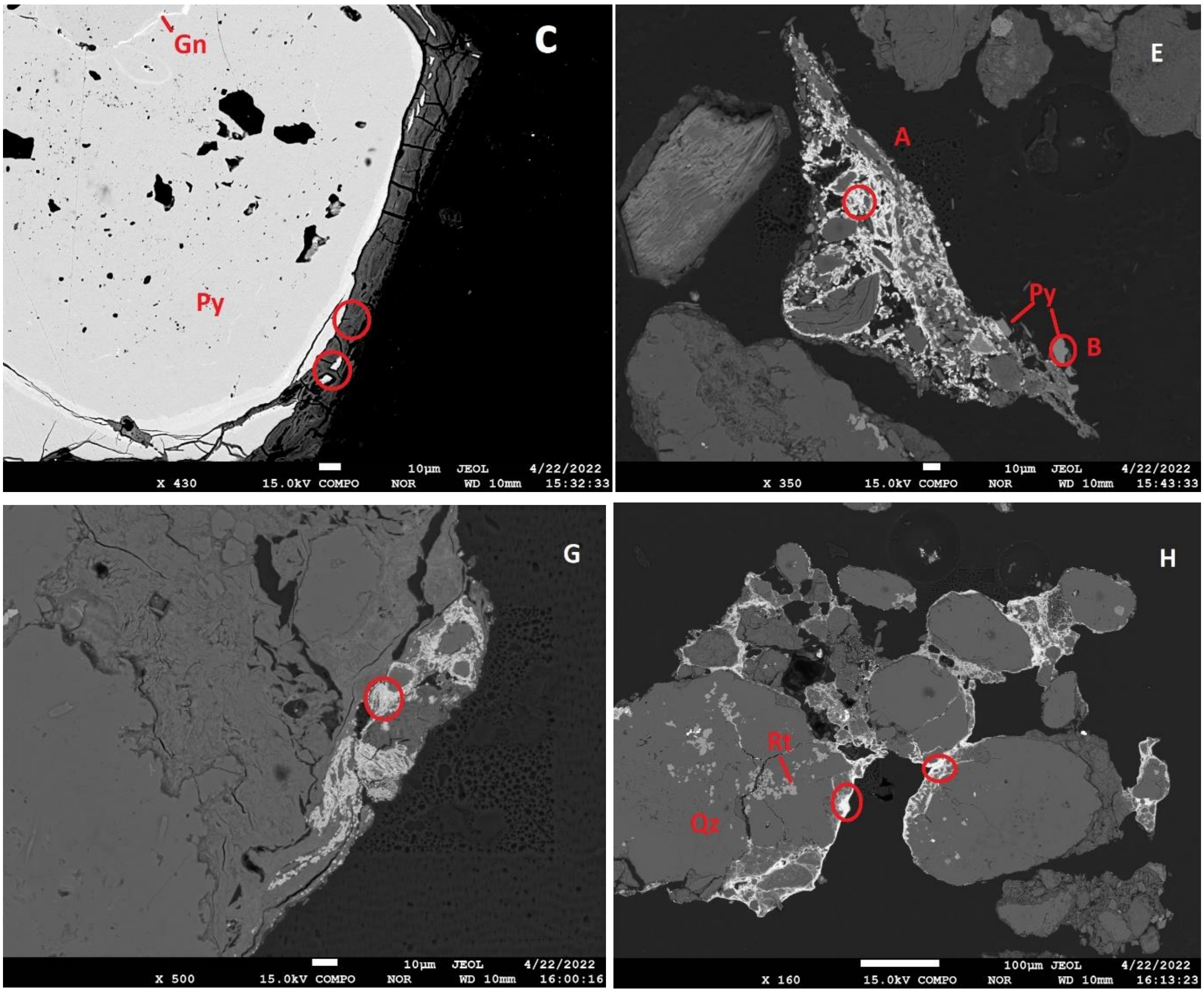

Fig. 19. Sample A2: **C.** HFO with As, **E$_A$.** Pb-Fe-Al-SO$_3$ phases with high P, Cu, As, **E$_B$:** As-Fe oxides with Al and Si, **G:** Pb-Fe sulfate, **H:** Cu-Pb-As oxides with high Y (Gn: Galena, Py: Pyrite, Qz: quartz, Rt: rutile)

In sample B4, the areas A-K (Fig. 20) were analyzed under the electron probe microanalyzer and those with the greatest mineralogical interest were A, B, C, and F (Fig. 21).

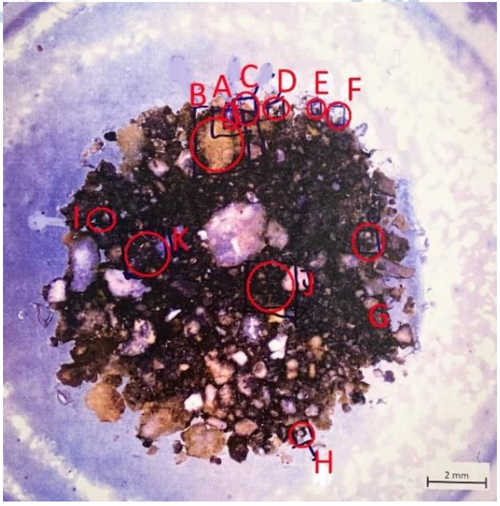

Fig. 20. Sample B4: The analyzed areas A-K.

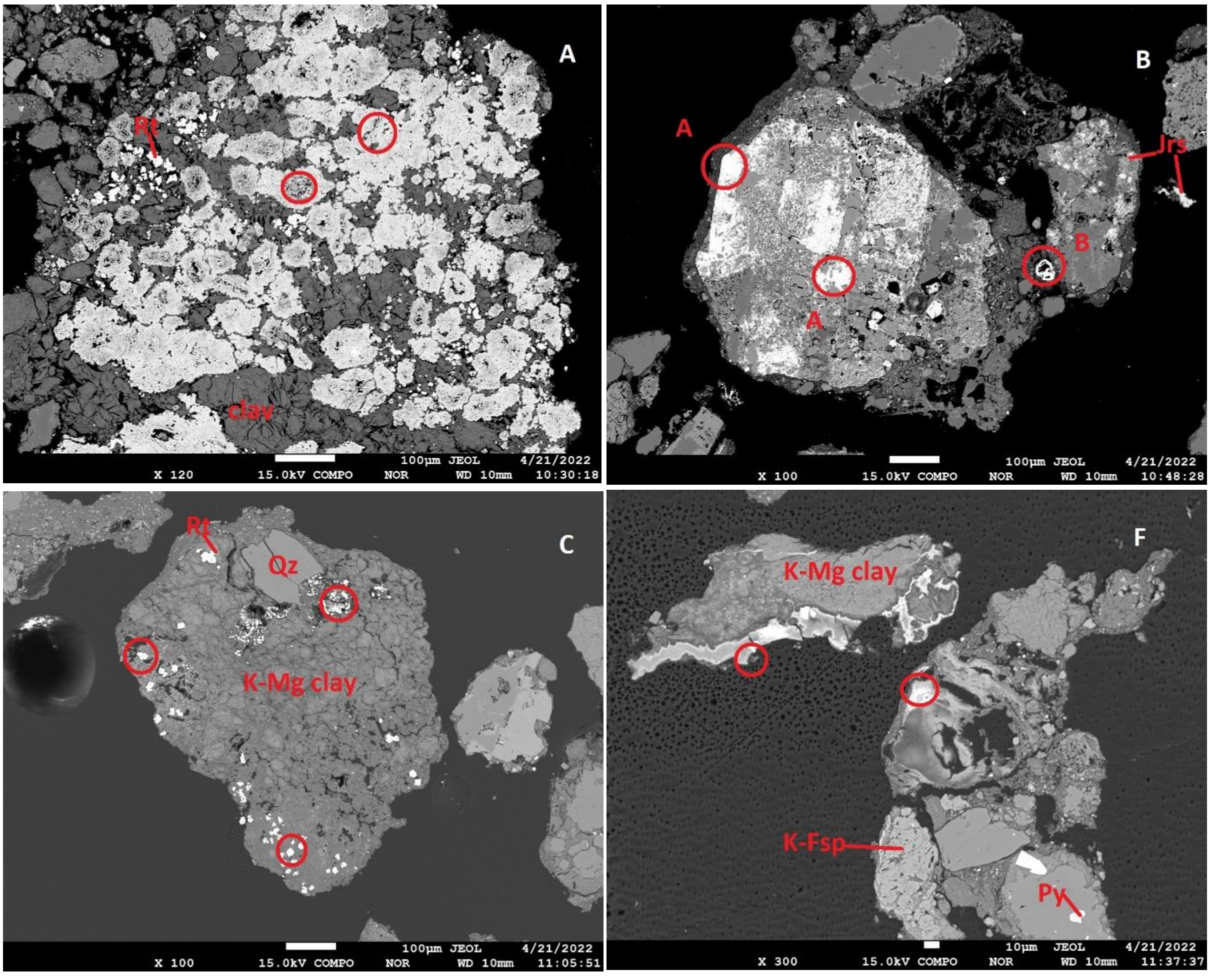

Fig. 21. Sample B4: **A.** Jarosite with low Sb and Pb, **B**$_A$**:** HFO with As and low Cu, **B**$_B$**:** Sb-Fe oxide, **C:** Pb-Fe-Al-SO_3 phases with high As, P, Cu, **F:** As-rich Al-HFO (Qz: Quartz, Fsp: Feldspar, Py: Pyrite, Jrs: Jarosite, Rt: Rutile).

In sample S, the areas A-M (Fig. 22) were analyzed under the electron microanalyzer and those with the most interesting secondary mineral phases were A, B, F, G, K, and M (Fig. 23).

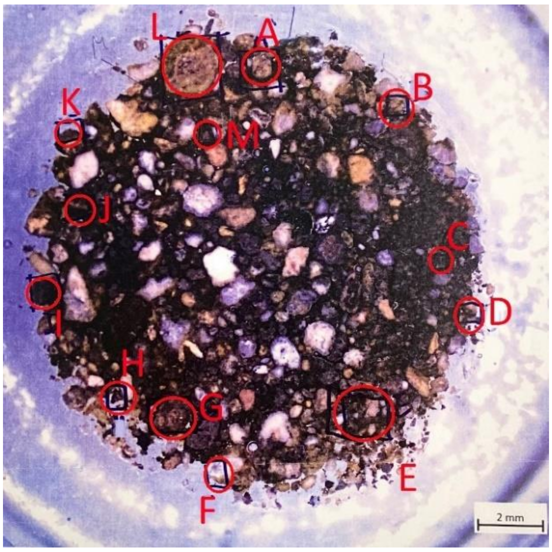

Fig. 22. Sample S: The analyzed areas A-M.

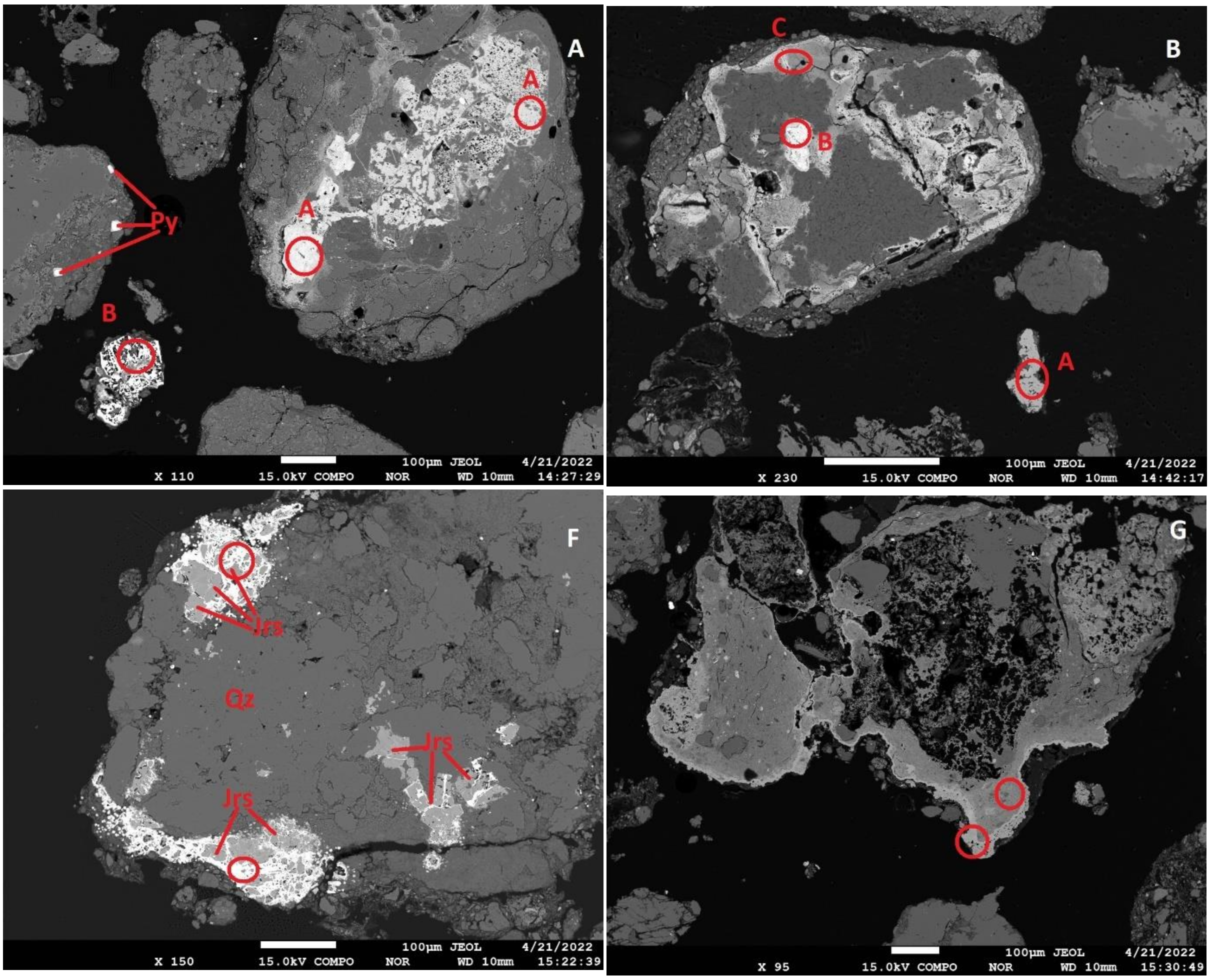

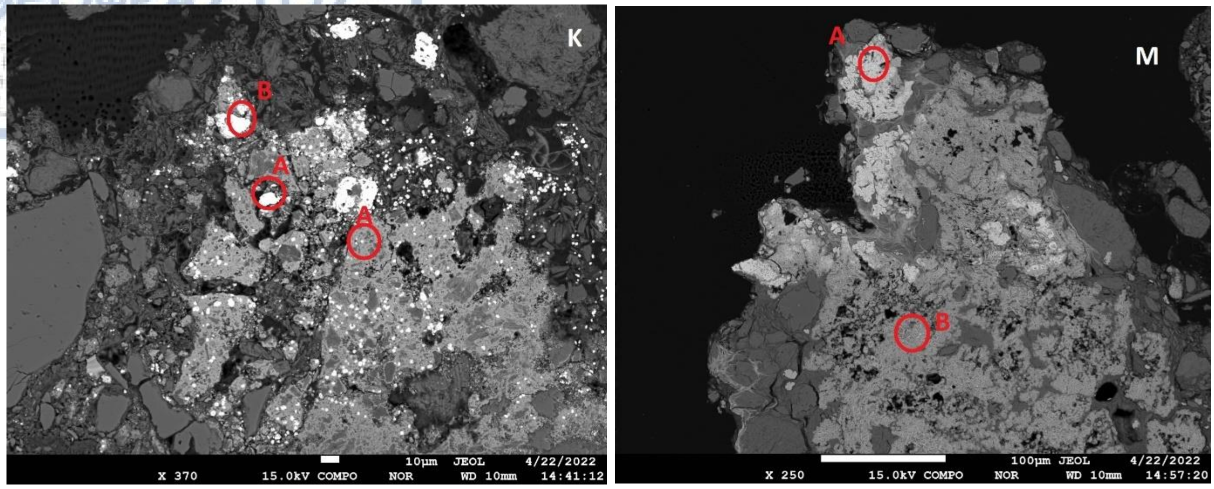

Fig. 23. Sample S: **A_A.** HFO, **A_B.** Zn-rich MHO, **B_A.** Jarosite with high S, K, Fe, **B_B.** HFO, **B_C.** TiO_2, **F.** Pb-Fe-Al-SO_3 phases with high P, Cu, **G.** HFO with clay (high Si and Al), **K_A.** Al-HFO with As, Sb, Cu, **K_B.** Pb-Fe-Al-SO_3 phases with high P, Cu, **M_A.** HFO_HMO with Zn, Sb, **M_B.** HFO with Cu (Qz: Quartz, Py: Pyrite, Jrs: Jarosite).

Total concentrations of the analyzed areas (%)

The total concentrations of the analyzed areas of the samples A2, B4, and S after the microprobe analysis are presented in tables 14, 15, and 16 respectively.

Tables 14A. 14B: Total concentrations in Sample A2 (sums <100% possibly because of the H_2O's presence, which can't be observed under the EPMA).

Sample A2 (A)	Al_2O_3	P_2O_5	As_2O_5	K_2O	CaO	SO_3	Sb_2O_5	TiO_2
	%							
C	5.997	0.047	1.85	0.005	0.209	7.089	0.215	0.014
C	6.71	0.02	2.679	0.017	0.176	8.523	0.18	0
E_A	15.375	0.054	9.546	2.112	0.098	10.988	1.113	0.054
E_B	10.757	0.5	21.521	0.87	1.558	0.765	5.294	0
G	5.029	0.226	0.059	2.595	0	22.067	0.218	0.01
H	5.554	0.078	29.495	0.086	0.698	3.531	0.937	0
H	4.98	0.191	30.692	0	0.529	2.681	1.163	0

Sample A2 (B)	PbO	Fe_2O_3	MnO	CuO	ZnO	Na_2O	SiO_2	MgO	Total
	%								
C	0.594	76.697	0	0.781	0.028	0.022	0.637	0.003	94.188
C	0.365	76.266	0.047	0.742	0	0	0.575	0.025	96.325
E_A	22.76	15.435	0.065	3.948	0.158	0	9.817	0.159	91.682
E_B	0.049	34.712	0.084	0.189	0	0.218	14.362	0	90.879
G	15.524	33.953	0.083	3.479	0.122	0.084	2.268	0.047	85.764
H	8.705	0.131	0.643	30.669	0.11	0	0.348	0	80.985
H	5.462	0.097	0.2	32.284	0.435	0	0.405	0	79.119

Tables 15A. 15B: Total concentrations in Sample B4 (sums <100% possibly because of the H_2O's presence, which can't be observed under the EPMA).

Sample B4 (A)	**Al_2O_3**	**P_2O_5**	**As_2O_5**	**K_2O**	**CaO**	**SO_3**	**Sb_2O_5**	**TiO_2**
%								
A	0.337	1.066	0	7.425	0	22.906	0.648	0.017
A	2.506	1.455	0.003	6.903	0	20.608	0.609	0.015
B_A	3.328	1.92	3.716	0.024	0.347	0.333	0.144	0.015
B_A	4.043	2.036	3.555	0.089	0.615	0.326	0.255	0
B_B	5.238	0.921	4.817	0.006	0	1.233	39.593	0
C	17.593	1.257	13.973	0.523	0.055	10.842	0.59	0.073
C	23.885	4.488	4.351	1.57	0.063	17.302	0.493	0.007
C	24.545	9.836	1.511	0.781	0.437	13.343	0.198	0
F	15.331	0.322	7.33	0.003	0.179	3.163	1.704	0
F	14.323	2.693	2.246	0.279	2.045	2.153	0.321	0.129

Sample B4 (B)	**PbO**	**Fe_2O_3**	**MnO**	**CuO**	**ZnO**	**Na_2O**	**SiO_2**	**MgO**	**Total**
%									
A	0.25	46.291	0	0.076	0.024	0.417	0.243	0.018	79.718
A	1.559	38.397	0.007	0.113	0	0.272	2.98	0.136	75.563
B_A	0	74.801	0.011	0.497	0	0	1.469	0.013	86.618
B_A	0	79.257	0.014	0.563	0	0	1.562	0.025	92.34
B_B	0.17	31.015	0.569	1.383	0	0.003	1.424	0	86.372
C	34.123	7.662	0	2.863	0	0	0.267	0	89.821
C	31.059	5.012	0.008	2.783	0	0	1.42	0	92.441
C	36.605	3.993	0.003	1.154	0.127	0	0.489	0	93.022
F	0	39.056	0	1.43	0	0	0.296	0	68.814
F	0.043	52.554	6.144	0.547	0.024	0	3.978	0.238	87.717

Tables 16A. 16B: Total concentrations in Sample S (sums <100% possibly because of the H2O’s presence, which can’t be observed under the EPMA).

Sample S (A)	Al_2O_3	P_2O_5	As_2O_5	K_2O	CaO	SO_3	Sb_2O_5	TiO_2
	%							
A_A	1.978	1.354	1.157	0.034	0.375	0.099	0.035	5.193
A_A	0.123	0.625	0.47	0.047	0.177	0.368	0	0.016
A_B	1.01	0.12	0	0.125	0.589	0.545	0.456	0.019
B_A	0.519	2.31	0.106	6.477	0	21.801	0.476	0.015
B_B	0.415	1.748	0.039	0.025	0.43	0.21	0.026	2.149
B_C	0.676	0.393	0.062	0.048	0.472	0.087	0	78.198
F	20.232	9.963	0	0.404	1.284	9.279	0.06	0
F	21.73	9.695	0	0.465	0.305	10.451	0.043	0
G	7.958	1.546	0.226	1.361	1.706	0.611	0.266	0.304
G	8.081	2.209	0.177	1.744	2.027	1.441	0.253	0.041
G	1.02	1.742	0.029	0.034	1.566	2.152	0.389	0
K_A	12.81	2.066	1.003	0.009	0.424	2.19	3.173	0.023
K_A	22.628	9.369	0	0.158	0.3	7.6	0.054	0
K_B	20.839	8.793	0.47	0.231	0.366	8.937	0.118	0
M_A	0.343	0.173	0.069	0.072	0.508	0.213	0.071	0.049
M_B	1.917	0.366	0	0.162	0.436	0.636	0.229	0.038

Sample S (B)	PbO	Fe_2O_3	MnO	CuO	ZnO	Na_2O	SiO_2	MgO	Total
	%								
A_A	0.059	74.39	0.067	0.032	0.263	0	2.761	0.185	87.982
A_A	0.063	84.975	0.018	0.03	0.071	0	2.511	0.063	89.557
A_B	8.015	0.517	44.284	1.518	26.1	0	0.744	0.079	84.121
B_A	0	46.12	0.016	0	0.039	0.537	0.744	0.016	79.176
B_B	0.01	86.412	0.119	0.005	0.076	0	1.539	0.285	93.488
B_C	0	4.111	0.026	0.016	0.05	0.011	0.946	0.075	85.171
F	36.06	1.663	0.077	2.713	0	0	2.135	0	83.87
F	37.789	1.257	0.055	2.51	0	0	1.52	0	85.82
G	0.072	46.705	0.03	0.097	0.461	0	13.551	0.729	75.623
G	0.024	50.331	0	0.03	0.353	0	16.947	0.832	84.49
G	0.049	66.67	0.036	0.062	0.383	0	6.064	0.266	80.462
K_A	0.309	68.485	0.046	1.367	0.17	0	2.632	0.107	94.814
K_A	36.387	6.058	0	1.702	0.144	0	0.134	0	84.534
K_B	35.037	6.263	0.058	2.405	0.198	0	0.19	0	83.905
M_A	1.978	39.483	36.847	0.48	6.469	0	0.75	0.094	87.599
M_B	0.469	69.75	3.092	1.599	2.245	0	3.053	0.286	84.278

7.3.2. Interesting secondary mineral phases determined by Electron Probe Microanalysis (EPMA)

Cu-Pb-As oxides with high Yttrium: Yttrium (Y) is a rare-earth element (REE) which is observed under the microscope (Fig. 19.H).

Pb-Fe-Al-SO_3 phase with high P, Cu, As: This phase belongs to the Beudantite Group of minerals, which belongs to the Alunite Supergroup. This phase is observed to all the three analyzed samples. The EPMA X-ray maps (Fig. 24) show the contents of the elements of this phase in sample S, F (Fig. 23.F).

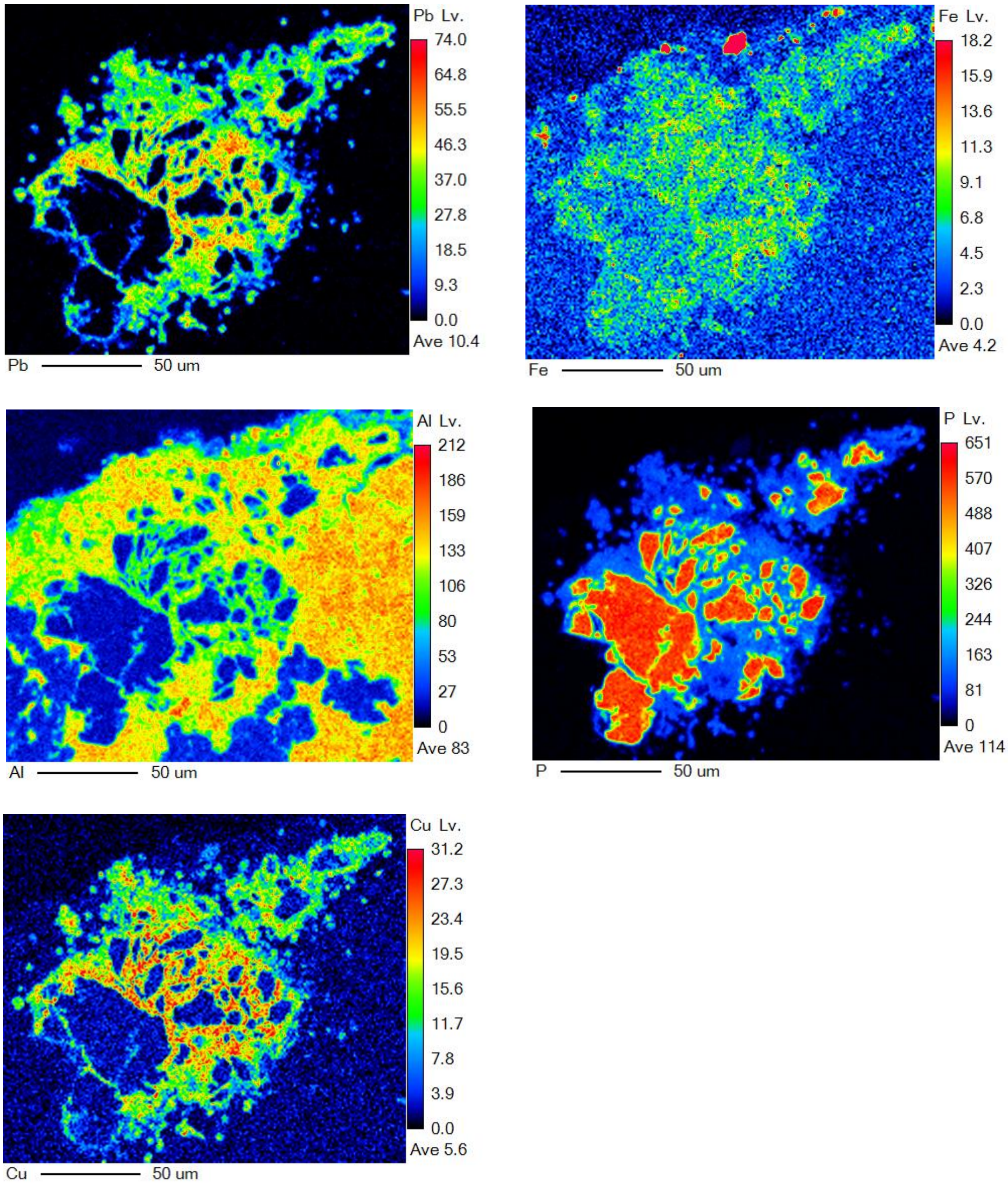

Fig. 24. Element maps of the Pb-phase in sample S, F (um).

Sb-Fe oxide: Tripuhytite, a secondary phase of Sb in sample B4, B_B.

HFO_HMO with high Zn and Sb: This phase is a mixture of Fe and Mn oxides and is observed in sample S, M_A. The EPMA X-ray maps (Fig. 25) show the contents of the elements of this phase in sample S, M_A (Fig. 23.M_A).

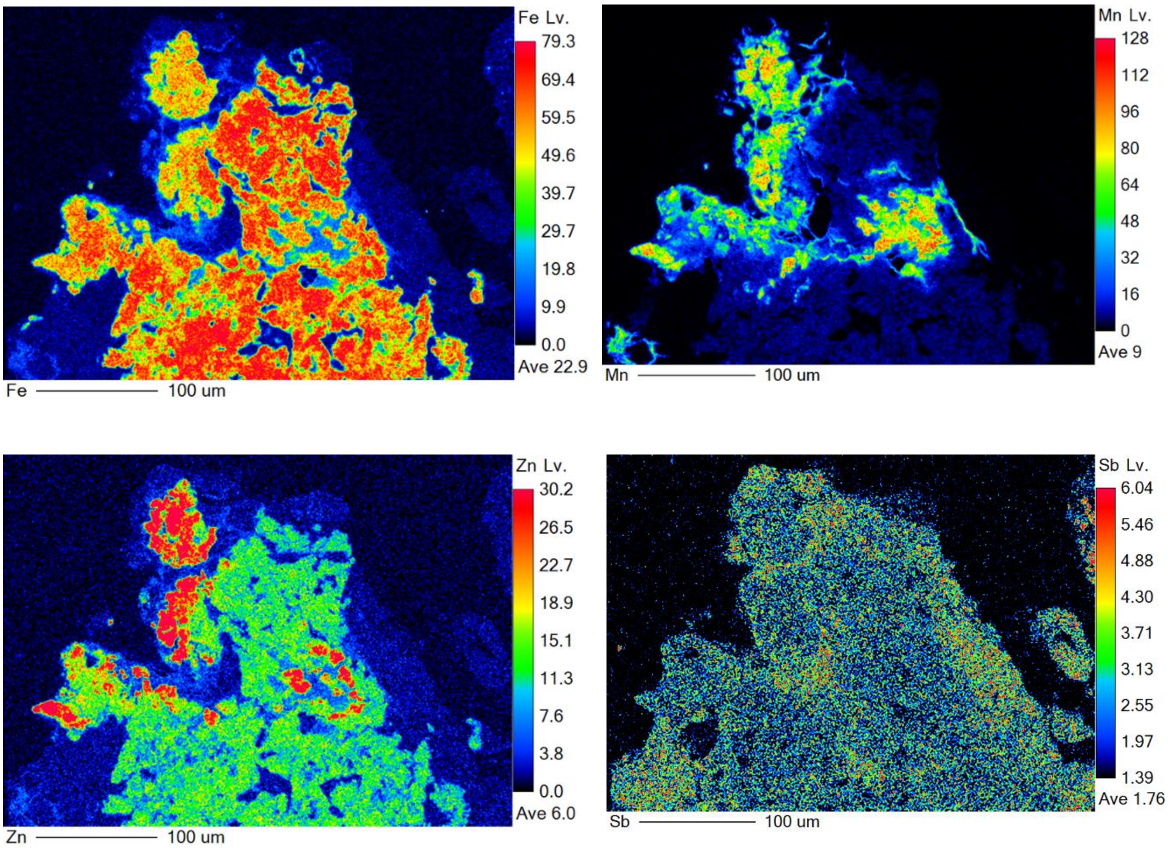

Fig. 25. Element maps of the HFO_HMO with high Zn phase in sample S, M_A (um).

Jarosite with Pb and low Sb: Jarosite is a basic hydrous sulfate of potassium (K) and ferric iron (Fe^{3+}). This phase was also detected by the XRD analysis (7.1.1.). The EPMA X-ray maps (Fig. 26) show the contents of the elements of this phase in sample B4, A (Fig. 21.A).

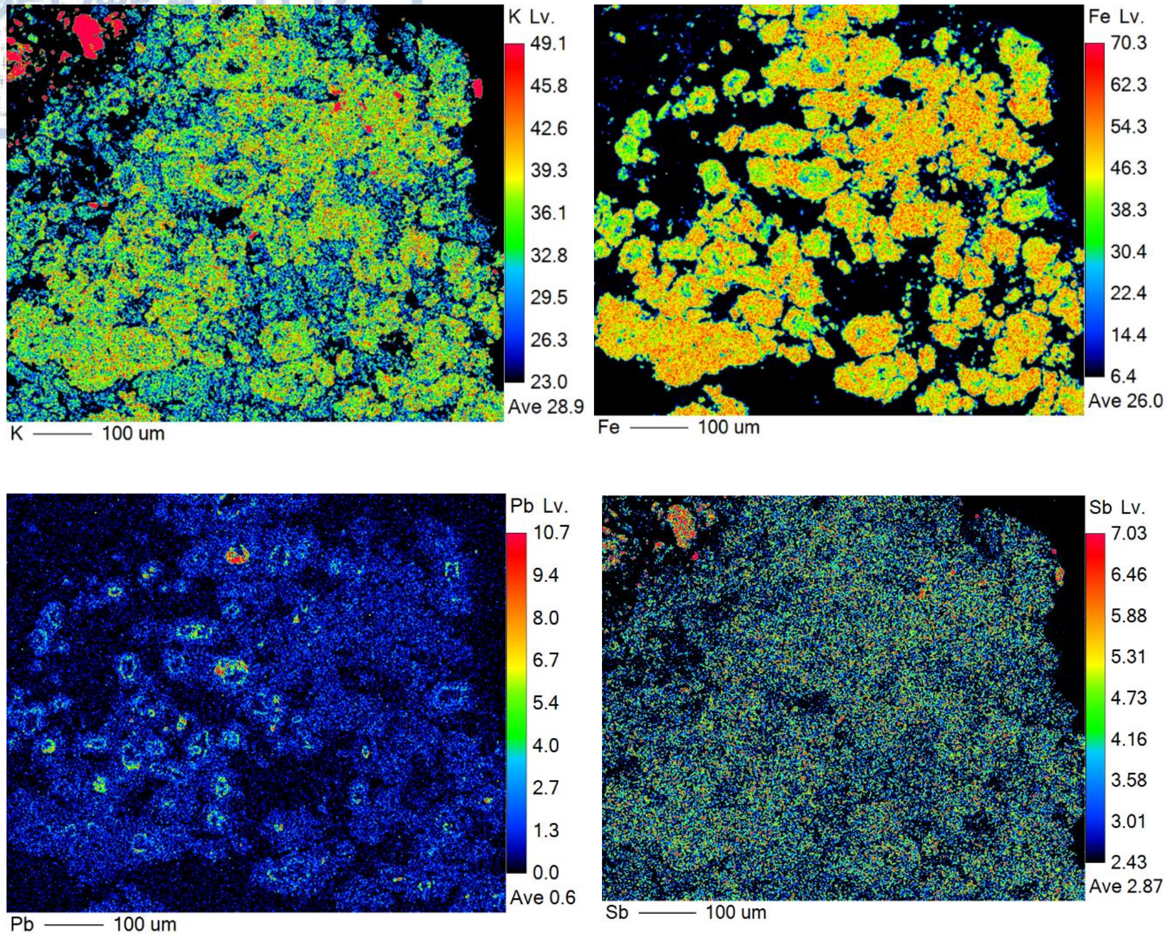

Fig. 26. Element maps of the jarosite phase in sample B4, A (um).

8. Conclusions

The global mean contents of trace elements in soils (Kabata-Pendias, 2011) include As (6.83 mg/kg), Cu (38.9 mg/kg), Pb (27 mg/kg), In (0.06 mg/kg), Sb (0.67 mg/kg), and Zn (70 mg/kg). In this study, the concentrations of these elements in the profiles A, B, and the sediment S were much higher than those averages. The application of ICP-OES and ICP-MS spectrometry showed the following mean contents. In the profile A, the mean contents are 229.4 mg/kg for As, 1338.6 mg/kg for Cu, 1734mg/kg for Pb, 6mg/kg for In, 329mg/kg for Sb, and 914.2mg/kg for Zn. In the profile B, the mean concentrations were extremely high too for As (449 mg/kg), Cu (880 mg/kg), Pb (766.5 mg/kg), In (2.635 mg/kg), Sb (443.25 mg/kg), and Zn (152.5 mg/kg). Finally, in the sediment S, the contents of these metals also exceeded the global mean contents for: As (252 mg/kg), Cu (649 mg/kg), Pb (630 mg/kg), In (0.48 mg/kg), Sb (181 mg/kg), and Zn (972 mg/kg).

Copper is an immobile element in soils and shows a relatively slight variation in total contents of the soil profiles. The common characteristic of Cu distribution in soil profiles is its accumulation in the top horizons. This phenomenon is an effect of various factors, mostly, because Cu is concentrated in surface soils, reflecting its bioaccumulation as well as its anthropogenic sources. In the other hand, Zn is a very mobile element during weathering processes and its easily soluble compounds are readily precipitated by reactions with carbonates, or it is absorbed by minerals and organic compounds, especially in the presence of sulfur anions. Cu and Zn sometimes interact because the factors controlling the mobility of Zn in soils are very similar to those related to Cu, but Zn appears to occur in more easily soluble forms.

Indium is likely to precipitate under conditions that form Fe and Mn hydroxides, and therefore it is associated with Fe-bearing minerals. It is often related to sulfide minerals (sphalerite, galena, chalcopyrite). In general, the In concentrations between 10-20 mg/kg in these minerals make them the main sources for mining it. However, it is often recovered from residues, during the production of Zn, Pb and Sn.

Lead sulfides oxidize slowly and have an ability to form carbonates and also to be fixed by clay minerals and hydroxides during weathering. Lead is the least mobile among the other trace metals in soils. The anthropogenic Pb in soils causes extremely hazardous to man and animals through the soil dust inhalation and the food chain.

Arsenic is an element highly associated with deposits of several metals and metalloids, and is a good indicator in geochemical prospecting surveys. Several As-oxide minerals result from the oxidation of sulfide mineralization. These are arsenates in which As is combined with metals like Fe, Pb, and Cu. The geochemical characteristics of Sb are closely related to those of As. Antimony is often associated with ore deposits of sulfide of other metals. It is easily adsorbed and that’s why it is rich in clay sediments and hydrous oxides. Antimony in high concentrations could be associated with nonferrous ore deposits and is likely to be a pollutant in industrial environments.

9. References

Arikas, K., Voudouris, P., (1998). Hydrothermal alterations and mineralizations of magmatic rocks in the southern Rhodope Massif, Acta Vulcanologica 10(2), 353-365.

Ashworth, K. L., Billet, M. F., Constantinidis, D., Demetriades, A., Katirtzoglou, C., Michael, C., (1988). Base metal mineralization in the Evros region Thrace, N. E. Greece, part of the Special Publication of the Society for Geology Applied to Mineral Deposits book series (MINERAL DEPOS.,volume 5), Berlin Heidelberg: Springer, pp. 169-181. https://doi.org/10.1007/978-3-662-02538-3_11

Bonev, N., Stampfli, G., (2008). Gabbro, plagiogranite, and associated dykes in the supra-subduction zone Evros Ophiolites, NE Greece, Geological magazine 146, 72-91. https://doi.org/10.1017/S0016756808005396

Caracciolo, L., Critelli, S., Cavazza, W., (2014). The Rhodope Zone as a primary sediment source of the southern Thrace basin (NE Greece and NW Turkey): evidence from detrital heavy minerals and implications for central-eastern Mediterranean palaeogeography. https://doi.org/10.1007/s00531-014-1111-9

Castaing, R., (1960). Electron Probe Microanalysis, Advances in Electronics and Electron Physics 13, 317-386. https://doi.org/10.1016/S0065-2539(08)60212-7

Dimou, E., Michael, K., Serment, R., (1994). Mineralogical composition of the epithermal-polymetallic ore of Pefka, Rhodope.

Dold, B., (2003). Speciation of the most soluble phases in a sequential extraction procedure adapted for geochemical studies of copper sulfide mine waste, Journal of Geochemical Exploration 80, 55–68. https://doi.org/10.1016/S0375-6742(03)00182-1

Drahota, P., Grösslová, Z., Kindlová, H., (2014). Selectivity assessment of an arsenic sequential extraction procedure for evaluating mobility in mine wastes. Analytica Chimica Acta 839, 34–43.

Drahota, P., Knappova, M., Kindlova, H., Culka, A., Majzlan, J., Mihaljevic, M., Rohovec, J., Veselovsky, F., Fridrichova, M., Jehlicka, Jan., (2016). Mobility and attenuation of arsenic in sulfide- rich mining wastes from Czech Republic, Science of the total environment, 192-203, http://dx.doi.org/10.1016/j.scitotenv.2016.03.079

Epp, J., (2016). 4 - X-ray diffraction (XRD) techniques for materials characterization, Materials Characterization Using Nondestructive Evaluation (NDE) Methods, 81-124. https://doi.org/10.1016/B978-0-08-100040-3.00004-3

Ettler, V., Jarosikova, A., Mihaljevic, M., Kribek, B., Nyambe, I., Kamona, F., Mapani, B., (2020). Vanadium in slags from smelting of African Pb-Zn vanadate ores: Mineralogy, extractability, and potential recovery, Journal of geochemical exploration, 106631. https://doi.org/10.1016/j.gexplo.2020.106631

Ettler, V., Mihaljevic, M., Drahota, P., Kribek, B., (2022). Cobalt-bearing copper slangs from Luanshya (Zambian Copperbelt): Mineralogy, geochemistry, and potential recovery of critical metals, Journal of geochemical exploration, 106987. https://doi.org/10.1016/j.gexplo.2022.106987

Kabata-Pendias, A., (2011). Trace elements in soils and plants, 4th edition.

Karimian, N., Johnston, S. G., Burton, E. D., (2017). Antimony and arsenic partitioning during Fe(II)- induced transformation of jarosite under acidic conditions. http://dx.doi.org/10.1016/j.chemosphere.2017.12.106

L.-E. Ricou, J.-P. Burg, I. Godfriaux & Z. Ivanov (1998). Rhodope and Vardar: the metamorphic and the olistostromic paired belts related to the Cretaceous subduction under Europe, Geodinamica Acta, 11:6, 285-309. https://doi.org/10.1080/09853111.1998.11105326

Marchev, P., Kaiser- Rohrmeier, M., Heinrich, C., Ovtcharova, M., Quadt, von A., Raicheva, R., (2005): Hydrothermal ore deposits related to post-orogenic extensional magmatism and core complex formation: The Rhodope Massif of Bulgaria and Greece, Ore Geology Reviews 27, 53-89. https://doi.org/10.1016/j.oregeorev.2005.07.027

Melfos, V., Voudouris, P., (2012). Geological, Mineralogical and Geochemical Aspects for Critical and Rare Metals in Greece, Minerals 2(4), 300-317. https://doi.org/10.3390/min2040300

Melfos, V., Voudouris, P., (2017). Cenozoic metallogeny of Greece and potential for precious, critical, and rare metals exploration, Ore Geology Reviews 89, 1030-1057. http://dx.doi.org/10.1016/j.oregeorev.2017.05.029

Michael, C. (2004). EPITHERMAL SYSTEMS AND GOLD MINERALIZATION IN WESTERN THRACE (NORTHERN GREECE). *Bulletin of the Geological Society of Greece*, *36*(1), 416–423. https://doi.org/10.12681/bgsg.16727

Naden, J, Kilias, S. P, Darbyshire, D. P. F., (2005). Active geothermal systems with entrained seawater as modern analogs for transitional volcanic-hosted massive sulfide and continental magmato-hydrothermal mineralization: The example of Milos Island, Greece, Geology, 541–544. https://doi.org/10.1130/G21307.1

Nesbitt, R. W., Billett, M. F., Ashworth, K. L., Deniel, C., Constantinides, D., Demetriades, A., Katirtzoglou, C., Michael, C., Mposkos, E., Zachos, S., Sanderson, D., (1988). The geological setting of base mineralization in the Rhodope region, northern Hellas, Mineral Deposits within the European Community, 499-514.

Nordstrom, D.K., (1977). Thermochemical redox equilibria of Zobell’s solution, Geochimica et Cosmochimica Acta 41, 1835–1841. https://doi.org/10.1016/0016-7037(77)90215-0

Pansu, M., Gautheyrou, J., (2006). Handbook of Soil Analysis: Mineralogical, Organic and Inorganic Methods. Springer-Verlag, Berlin, Heidelberg 2006. https://doi.org/10.1007/978-3-540-31211-6

Papanikolaou, D., Panagopoulos, A., (1981). On the structural style of the Southern Rhodope, Greece, Geologica Balcanica 11, 13-22.

Passos, E. de A. et. Al., (2010). Assessment of trace metals contamination in estuarine sediments using a sequential extraction technique and principal component analysis, Microchemical Journal 96, 50-57. https://doi.org/10.1016/j.microc.2010.01.018

Pirajno, F., (2009). Hydrothermal Processes and Mineral Systems, Springer Science and Business Media LLC.

Tilley, D., (2021). Epithermal gold deposits, Geology for investors.

Tombros, S., Seymour, St. K., Williams-Jones, A. E., Spry, P.G., (2007). The Genesis of Epithermal Au-Ag-Te Mineralization, Panormos Bay, Tinos Island, Cyclades, Greece, Economic Geology 102(7):1269-1294. https://doi.org/10.2113/gsecongeo.102.7.1269

Ure, A.M., (1996). Single extraction schemes for soil analysis and related applications, Science of the Total Environment 178, 3–10. https://doi.org/10.1016/0048-9697(95)04791-3

Varshneya, K. A, Mauro, J. K., (2019). Fundamentals of Inorganic Glasses (Third edition). https://doi.org/10.1016/C2017-0-04281-7

Voudouris, P., Repstock, A., Spry P.G., Frenzel, M., Mavrogonatos, C., Keith, M., Tarantola, A., Melfos, Va., Tombros, St., Zhai, D., Cook, N. J., Ciobanu, C. L., Schaarschmidt, A., Rieck, B., Kolitsch, U., Falkenberg, J., (2022). Physicochemical constraints on indium-, tin-, germanium-, gallium-, gold-, and tellurium-bearing mineralizations in the Pefka and St Philippos polymetallic vein- and breccia-type deposits, Greece, Ore Geology Reviews, 104348. https://doi.org/10.1016/j.oregeorev.2021.104348

Warr, L.N., (2021). IMA–CNMNC approved mineral symbols, Mineralogical Magazine 85, 291–320. https://doi.org/10.1180/mgm.2021.43

White, N. C., Hedenquist, J. W., (1989). Epithermal environments and styles of mineralization: Variations and their causes, and guidelines for exploration, Journal of geochemical exploration 36, 445-474. https://doi.org/10.1016/0375-6742(90)90063-G